Nanoscale

ROYAL SOCIETY OF CHEMISTRY

REVIEW

View Article Online
View Journal | View Issue

Cite this: *Nanoscale*, 2023, **15**, 8900

Progress and prospectives of solution-processed kesterite absorbers for photovoltaic applications

Lijing Wang, Yufei Wang, Zhengji Zhou, * Wenhui Zhou, Dongxing Kou, Yuena Meng, Yafang Qi, Shengjie Yuan, Litao Han and Sixin Wu*

Solar cells based on emerging kesterite $Cu_2ZnSn(S,Se)_4$ (CZTSSe) materials have reached certified power conversion efficiency (PCE) as high as 13.6%, showing great potential in the next generation of photovoltaic technologies because of their earth-abundant, tunable direct bandgap, high optical absorption coefficient, environment-friendly, and low-cost properties. The predecessor of CZTSSe is Cu(In,Ga) Se_2 (CIGS), and the highest PCE of CIGS fabricated by the vacuum method is 23.35%. However, the recorded PCE of CZTSSe devices are fabricated by a low-cost solution method. The characteristics of the solvent play a key role in determining the crystallization kinetics, crystal growth quality, and optoelectronic properties of the CZTSSe thin films in the solution method. It is still challenging to improve the efficiency of CZTSSe solar cells for future commercialization and applications. This review describes the current status of CZTSSe solar cell absorbers fabricated by protic solvents with NH (hydrazine), protic solvents with SH (amine–thiol), aprotic solvents (DMSO and DMF), ethylene glycol methyl ether-based precursor solution method (EGME), and thioglycolic acid (TGA)-ammonia solution (NH_3H_2O) deposition methods. Furthermore, the performances of vacuum-deposited devices and solution-based processed devices are compared. Finally, the challenges and outlooks of CZTSSe solar cells are discussed for further performance improvement.

Received 14th January 2023,
Accepted 12th April 2023

DOI: 10.1039/d3nr00218g

rsc.li/nanoscale

1. Introduction

New renewable energy provides a novel strategy to alleviate the energy crisis and environmental pollution, in which photovoltaic power generation technology provides a feasible and important technical support for achieving green environmental protection, energy saving and emission reduction.[1–3] Kesterite $Cu_2ZnSn(S,Se)_4$ (CZTSSe) solar cells, as the most

Key Laboratory for Special Functional Materials of Ministry of Education, National & Local Joint Engineering Research Centre for High-efficiency Display and Lighting Technology, School of Materials, Collaborative Innovation Centre of Nano Functional Materials and Applications, Henan University, Kaifeng, 475004, China.
E-mail: zzj@henu.edu.cn, wusixin@henu.edu.cn

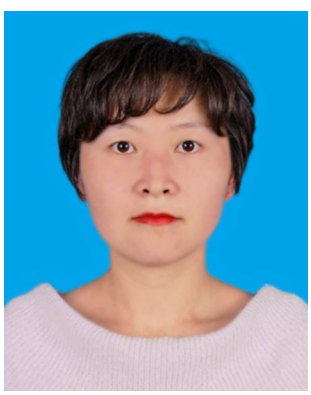

Lijing Wang

Lijing Wang received her B.S. degree in materials science and engineering in 2016 and M.S. degree in Materials in 2019 from the Henan University of Technology. She is currently a Ph.D. candidate under the supervision of Professor Sixin Wu and Zhengji Zhou at Henan University. Her research work mainly focuses on the fabrication of high efficiency CZTSSe thin film solar cells.

Zhengji Zhou

Zhengji Zhou received both the B.S. degree and Ph.D. degree from Henan University. Currently, he is a professor at Key Lab for Special Functional Materials of Ministry of Education, Henan University. His major is condensed matter physics and materials and his main interest is concerned with the research of emerging solar energy materials and photovoltaic devices.

promising photovoltaic star, show great potential in the next generation of photovoltaic technologies because of their earth-abundant, tunable direct bandgap, high optical absorption coefficient, environment-friendly, and low-cost properties.[4–12] CZTSSe solar cells are inherited from its predecessor of Cu(In, Ga)(S,Se)$_2$ (CIGS). However, the current highest power conversion efficiency (PCE) of CIGS devices is 23.35%, which was achieved by vacuum method[13,14] whereas the recorded PCE of CZTSSe devices were obtained using solution processing techniques. Vacuum methods require extremely high energy input, huge capital investment and excessive operating costs.[15–17] In addition, low yields, process complexity, revenue and material utilization hinder the transition of high-performance devices from laboratory to large-scale commercial production.[18–20] Fortunately, the solution method is considered to have broad development prospects and huge application potential because of its advantages of low cost, easy large-area preparation and ideal PCE.[21–23] In 2021, the PCE of 13.0% was achieved by Xin's group with dimethyl sulfoxide (DMSO)-based processing.[24] In addition, Meng *et al.* further improved the efficiency to 13.6% by employing the solution method.[4] Notably, the certified efficiency of the CZTSSe solar cell fabricated by applying the solution method broke the highest efficiency of 12.62% created by Kim *et al.* using the vacuum method.[25,26]

At present, the fabrication of CZTSSe absorbers generally involves the following processes by solution processing: (i) applying a wet precursor layer to the substrate and (ii) heat treating the precursor layer under sulfur and/or an inert atmosphere to obtain the final polycrystalline absorbers.[27,28] The hydrazine-based precursor solution is the most successful method for the preparation of CZTSSe solar cells in the solution method developed by IBM in 2010,[29] which achieved the highest certified conversion efficiency of 12.6% in 2013; this record efficiency has been maintained for many years.[30] However, hydrazine solvents are not only highly toxic and explosive but also some countries and regions explicitly restrict their transportation and application. The limitations of hydrazine solvents have significantly stimulated the rapid development and widespread use of solution methods in non-hydrazine solvent systems. Currently, various environmentally friendly, safe, stable and high-efficiency solvent systems have been successfully developed, including dimethyl sulfoxide (DMSO), *N*,*N*-dimethylformamide (DMF), ethylene glycol methyl ether (EGME), thioglycolic acid and ammonia (TGA), and ethylenediamine/ethanedithiol system (EN/EDT).[31–35] Both vacuum method and solution processes have resulted in significant improvements in CZTSSe device performance,[36–39] and the development of PCE evolution is shown in Fig. 1. A typical schematic diagram of CZTSSe thin-film solar cells prepared by solution is shown in Fig. 2. Several solution processes have resulted in significant improvements in CZTSSe device performance compared with the vacuum method. However, the highest efficiency of CZTSSe manufactured from solution processed (13.6%) is significantly lower than the theoretical limit of about 32% predicted by the Shockley–Queisser model.

Herein, we summarize the advanced research progress made in the fabrication of high-quality and high-efficiency CZTSSe solar cells using the solution method. Specifically, the route origins and dissolution chemistry of different solvents are summarized in detail. Additionally, some critical insights are presented on the current challenges and opportunities of CZTSSe solar cells with various solvents for future commercial production. This review not only provides important perspectives on the development of high-performance CZTSSe solar cells but is also essential for laboratory-scale research on the large-scale manufacturing production of CZTSSe solar cells.

2. Protic solvents with NH

2.1. Hydrazine (N_2H_4)

Solvent systems, which can dissolve bulk chalcogenide materials to provide precursor solutions, are valuable for the fabrication of kesterite solar cells. Subsequently, these precur-

Sixin Wu

Sixin Wu received his Ph.D. degree in Shanghai Institute of Optics and Fine Mechanics in 1999. From 2000 to 2006, he worked as postdoctoral researcher at Tohoku University and National Institute for Materials Science, Tsukuba, Japan, University of Texas at Arlington, USA. He is currently a professor at the Key Laboratory for Special Functional Materials of the Ministry of Education, Henan University, China. At present, he is mainly engaged in the research of inorganic thin film photovoltaic devices.

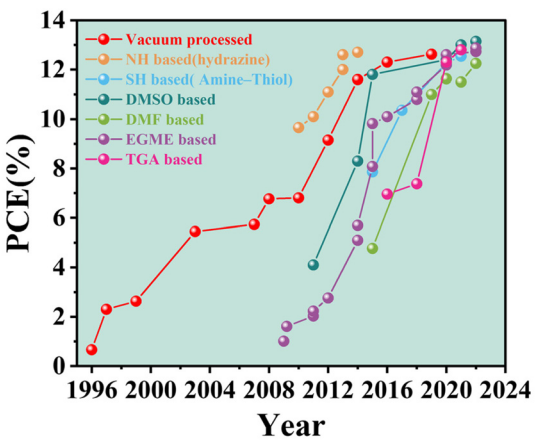

Fig. 1 The power conversion efficiency evolution of $Cu_2ZnSn(S,Se)_4$ Solar Cells.

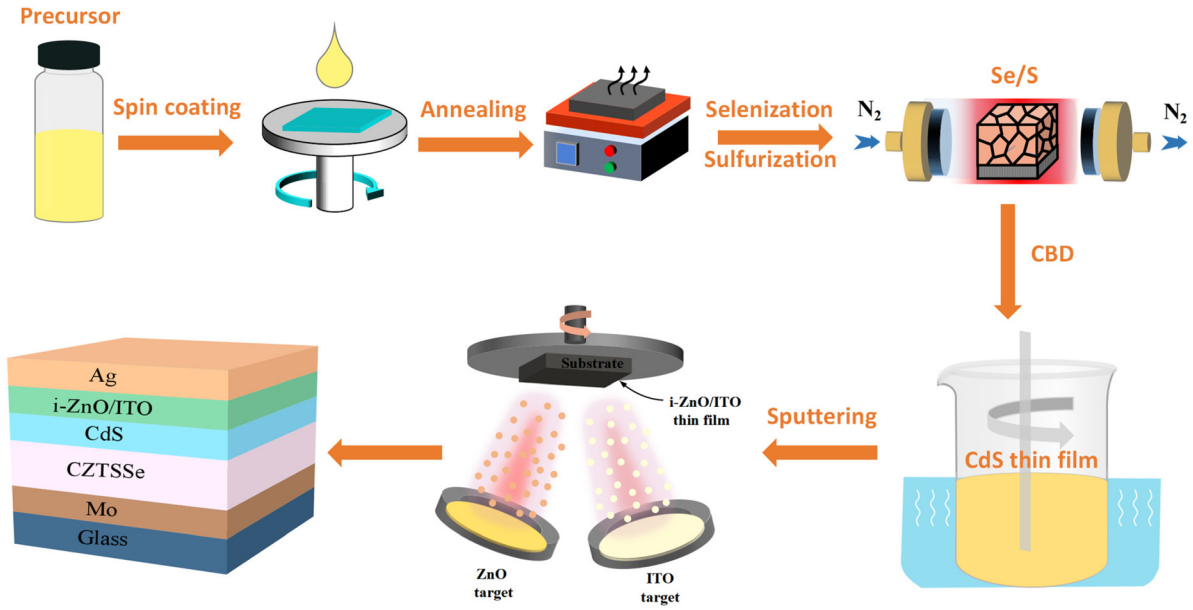

Fig. 2 Schematic illustration of the solution fabrication process of CZTSSe solar cells.

sor solutions can be processed into pure phase thin films. Consequently, Mitzi *et al.* first reported the solubility of hydrazine (N_2H_4) to dissolve a series of bulk chalcogenide compounds ($SnSe_{2-x}S_x$, In_2Se_3, GeS_2, $GeSe_2$, Cu_2S, Sb_2Se_3, Sb_2Te_3, $CuInSe_2$, $Cu(In_{1-x}Ga_x)Se_2$, $CuInTe_2$, Ga_2Se_3, KSb_5S_8, ZnTe, LiA_5S_2, and MoS_2).[40–43] The hydrazine solvent is carbon-free and volatile, providing the following characteristics for the preparation of kesterite thin films: (i) can dissolve many chalcogenide compounds, (ii) high solubility to sulfides, (iii) atmospheric pressure deposition pathway to reduce selenium and sulfur loss, and (iv) can be completely volatile without introducing impurity elements (Cl, C, O, and binary oxides).[44,45] Hydrazine solvent provides a feasible development strategy for kesterite semiconductor thin film materials and nanomaterials. However, hydrazine also has some disadvantages, greatly limiting its application in photovoltaics: (i) high toxicity and (ii) flammability and explosive.[46] In addition, some countries and regions explicitly restrict the transport and use of hydrazine. Therefore, the successful application of hydrazine solvent in photovoltaics needs reasonable operation and safe prevention. Notably, record PCEs of 12.6% (certified cell efficiencies) were reported from hydrazine molecular inks in 2013 (Table 1).[30]

2.2. PV applications for hydrazine-based routes

For high-efficiency CZTSSe solar cells, the key is to obtain high-quality absorbers.[47–54] The hydrazine-based precursor solution method was developed by the T. J. Watson Research Center of IBM Company (IBM T. J. Watson Research Center), which has been proved to be one of the most successful technologies for CZTSSe solar cells, both theoretically and experimentally. In 2008, the group of Mitzi was the first to apply this method to CIGS solar cells and obtained the first thin film solar cell with 10% PCE, which was the highest PCE of all solution methods for the preparation of absorber layers at that time.[42] In early 2010, the group similarly used hydrazine solution to obtain CuS/Se, SnS/Se and ZnS/Se (N_2H_2) particles and prepared CZTSSe thin films with a PCE of 9.66% (Fig. 3a).[29] Subsequently, the group achieved a PCE of 10.1% and proved that key recombination of CZTSSe devices from the main interface, short minority carrier lifetime and high series resistance.[55] In 2012, they used a hydrazine-based mixed particle thin film deposition method and optimized strategies to improve the PCE of CZTSSe solar cells, including (i) introducing 40% Ge to obtain 9.14% CZTSe solar cells[56] and (ii) changing the concentration of sulfur during heat treatment can not only regulate the band gap but also modify the interface layer between Mo/CZTSSe, improving FF and J_{SC}. Ultimately, the certification efficiency reached 11.1% (Fig. 3b).[57] Furthermore, the reaction pathway for the preparation of $Cu_2ZnSn(Se,S)_4$ absorber materials from liquid-phase hydrazine-based precursor inks and the role of sulfur in solution-processed $Cu_2ZnSn(S,Se)_4$ and its effect on defect properties were studied by Yang *et al.*[58,59]

However, zinc, zinc sulfides or zinc selenides cannot be directly dissolved even though the hydrazine solution has a super solubility, ultimately obtaining a hybrid solution with ZnSe particles and other molecular precursors rather than a precursor solution at the molecular level. Based on these technical barriers, Yang *et al.* obtained a true solution of zinc by dissolving the zinc powder in hydrazinic acid ($NH_2NHCOOH$). Then, a complexing agent was obtained by the reaction of solid CO_2 with hydrazine, and successfully solved the problem of dissolution of zinc, obtaining a homogeneous CZTS precursor solution at the molecular level, as shown in Fig. 3d.[61] Although this study achieved only a PCE of 8.08%, it can still

Table 1 A selected summary of precursor ink formulations, heat treatments, and device performances for $Cu_2ZnSn(S,Se)_4$ solar cells using hydrazine-based solution-deposited absorbers. PCE is the total area unless otherwise stated

Year	Solar cell	Molecular ink	Dissolution condition	Heat treatments	Area [cm^2]	V_{OC} [mV]	J_{SC} [mA cm^{-2}]	FF [%]	PCE [%]	Institute	Ref.
2010	CZTSSe	Cu_2S-S, SnSe-Se in N_2H_4, ZnSe (N_2H_4) particles were formed *in situ* by adding zinc powder to tin solution	N_2, glove box	Annealed (540 °C)	0.45	516	28.6	65	9.66[a,b]	IBM	29
2011	CZTSSe	Cu_2S-S in N_2H_4, Zn-SnSe-Se in N_2H_4	N_2, glove box	Annealed (540 °C)	0.45	517	30.8	63.7	10.1[a,b]	IBM	55
2012	CZTSe	Cu_2S-S in N_2H_4, Zn-SnSe and $GeSe_2$(Ge-substituted)-Se in N_2H_4	N_2, glove box	Annealed (540 °C)	0.45	476	31.8	60.4	9.14[a]	IBM	56
2012	CZTSSe	Cu_2S-S in N_2H_4, Zn-SnSe-Se in N_2H_4 – ZnSe (N_2H_2)	N_2, glove box	Annealed (500 °C)	0.45	459.8	34.5	69.8	11.1[a,b]	IBM	57
2012	CZTSSe	Zn in $NH_2NHCOOH$ + N_2H_4, Cu_2S-S in N_2H_4, SnS_2-S in N_2H_4	Stirring	Annealed (250–350 °C + 500 °C)	0.12	409	32.25	61	8.08[a,c,e]	UCLA	61
2013	CZTSSe	Cu-constituent, Sn-constituent, and Zn-constituent were dissolved in hydrazine	N_2, glove box	Annealed (500 °C)	0.1	406	30.5	59.55	7.4[e]	UCLA	59
2013	CZTSSe	Cu_2S-S in N_2H_4, Zn-SnSe-Se in N_2H_4 - ZnSe (N_2H_4)	N_2, glove box	Annealed (500 °C)	0.45	498	34.8	69.4	12[b]	IBM	60
2013	CZTSSe	Zn in $NH_2NHCOOH$ + N_2H_4, Cu_2S-S in N_2H_4, SnS_2-S in N_2H_4	N_2, glove box	Annealed (500 °C)	0.42	513.4	35.2	69.8	12.6[b]	IBM	30
2014	CZTSSe	Cu + S in hydrazine solution, Zn + Sn + Se in anhydrate hydrazine solution (two days at ambient temperature), and the Cu + S solution was injected into the vial containing Zn + Sn + Se precursor	N_2, glove box	Annealed (500 °C)	0.45	461	27.5	50.3	6.4	HUST[d]	62
2014	CZTSSe	Zn in $NH_2NHCOOH$ + N_2H_4, Cu_2S-S in N_2H_4, SnS_2-S in N_2H_4	N_2, glove box	Annealed (500 °C)	0.42	471	37.1	70.3	12.7 (12.3[b])	IBM	63

[a] Cells with ARC. [b] Certified cell efficiencies. [c] University of California Los Angeles (UCLA). [d] Huazhong University of Science and Technology (HUST). [e] Active area.

lay a foundation for further improving the efficiency of CZTSSe solar cells prepared by applying the hydrazine solution method. Subsequently, Winkler *et al.* developed the ultra-thin CdS buffer layer and transparent conductive layer (TCO) with a total thickness of about 50 nm, improving the transmittance of the CZTSSe absorbers, and the certified efficiency from 11.1% to 12.0% (Fig. 3c) because of the significant improvement in J_{SC}.[60] In addition, Mitzi *et al.* used the hydrazine-based pure solution method proposed by Yang *et al.* in 2012. They optimized not only the transparent conductive oxide (TCO) but also the CdS layer thickness, maximizing the photon transmission rate of the absorber layers using the hydrazine pure solution method to improve the bulk phase quality of CZTSSe films. The top view and cross-sectional view of the SEM images are shown in Fig. 3e and f, respectively.[30] The results show that a high-quality CZTSSe layer with homogeneous pinhole-free and large grain size was obtained, resulting in a champion efficiency of the CZTSSe photovoltaic device with a certified world record of 12.6%, which was maintained for a long time. In 2014, Tang *et al.* proposed a simple and effective sulfurization process to optimize the surface composition of the CZTSSe absorber with the well-built phase and large-grained films, but the efficiency of the device was only 6.4%.[62] Based on the previous studies, Mitzi's group proposed a double N buffer layer (In_2S_3/CdS) to solve the V_{OC}-deficit problem by optimizing the buffer layer structure, and they obtained the CZTSSe solar cell with V_{OC}-deficit less than 600 mV for the first time; finally, 12.7% efficiency was obtained (independently certified at 12.3% efficiency).[63]

As an ideal solvent without carbon and oxygen, hydrazine can also effectively dissolve metal and chalcogenide compounds for high efficiency CZTSSe solar cells. A certified record efficiency of 12.6% for CZTSSe solar cells was achieved from the hydrazine solution, and this record efficiency was maintained for many years. Moreover, the decomposition products of the preparation process are clean N_2, NH_3 and H_2, reducing the introduction of harmful impurities. In addition, the CZTSSe absorbers were mainly composed of large CZTS grains because of the hydrazine solvent without carbon. However, the hydrazine solvent is highly toxic and explosive and is suitable only for experimental research. Therefore, it is urgent to explore and develop other low-toxic and stable green solvents for commercial development.

3. Protic solvents with SH

3.1. Amine–thiol

To solve the problems of toxicity and safety of hydrazine solvents, it is urgent to develop a solvent with hydrazine solvation ability and volatility. A novel binary solvent mixture composed of 1,2-ethanedithiol and 1,2-ethylenediamine was reported by Brutchey's group at the University of Southern California (USC), which can dissolve large amounts of chalcogenides at

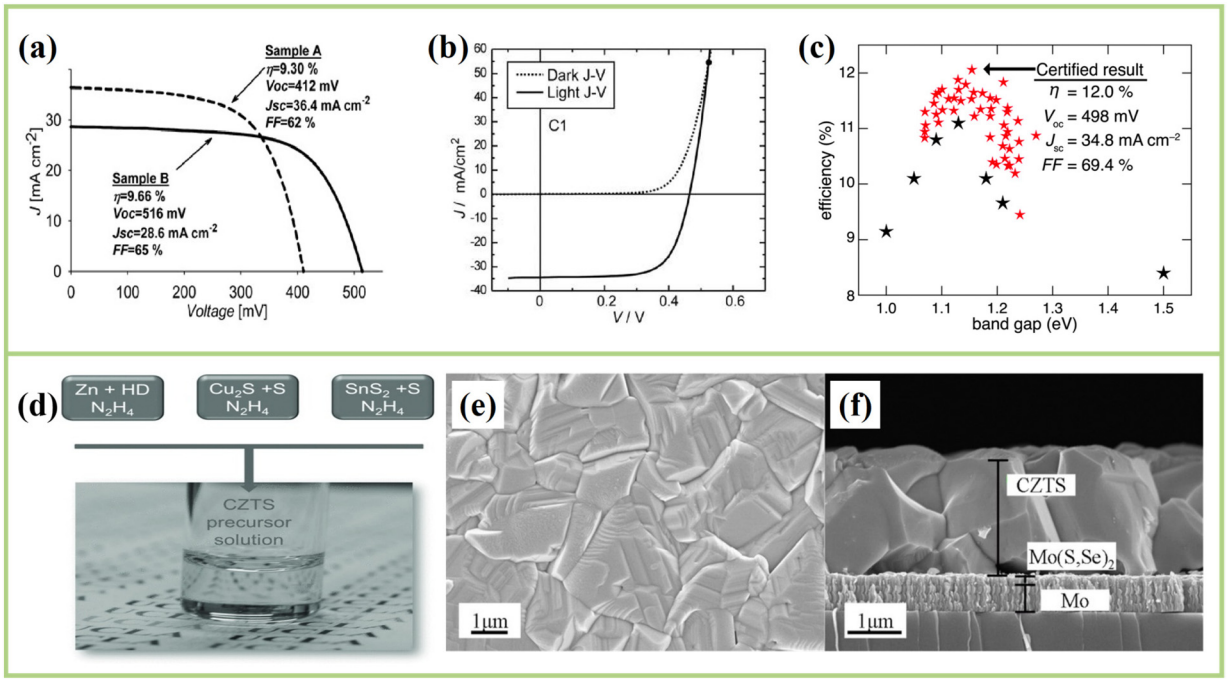

Fig. 3 (a) *J–V* curves of the certified efficient CZTSSe solar cells by Mitzi for the first time using a hydrazine solvent.[29] Copyright © 2010 WILEY-VCH Verlag GmbH & Co. KGaA. (b) *J–V* characteristics for the 11.1% champion cell.[57] Copyright © 2012 WILEY-VCH Verlag GmbH & Co. KGaA. (c) *J–V* characteristic of the 12.0% certified device.[60] Copyright © 2014 Royal Society of Chemistry. (d) Photographs of the hydrazine CZTS precursor solution prepared by Yang's synthesis through the reaction of metallic zinc and hydrazinocarboxylic acid (HD) derived from hydrazine and carbon dioxide.[61] Copyright © 2012 WILEY-VCH Verlag GmbH & Co. KGaA. (e) Top-view[30] and (f) cross-sectional view SEM images of the 12.6% record device.[30] Copyright © 2013 WILEY-VCH Verlag GmbH & Co. KGaA.

room temperature and ambient pressure.[64] Most ideal precursor materials are metal elements and metal sulfur for kesterite photovoltaic (PV). Preparing a precursor solution containing only the target element can exclude the influence of impurity atoms on device performance. Interestingly, the mixed solvent of 1,2-ethanedithiol and 1,2-ethylenediamine (EDT-EN) can not only dissolve Cu, Zn, and Sn metal elements but also S and Se non-metal elements.[44] The absorbers manufactured by this novel solvent also have the following advantages: (i) low boiling point, volatile solvent, the boiling point of ethylenediamine is 117 °C and ethylenedithiol is 146 °C, (ii) it is easy to synthesize single crystal nanoparticles, and (iii) no impurity atoms, (iV) preparation of high-quality precursor films. Successfully, a record PCE of 12.54% (Cells with ARC) was reported from amine–thiol molecular inks in 2021 (Table 2).[65] Although the toxicity of amine–thiol is slightly lower than that of hydrazine, the significant toxicity of amine and thiol still drives the development of green solution systems for the fabrication of chalcogenide semiconductors.[66] Currently, the developed low-toxic solvents are DMSO, DMF, EGME and TGA. A more detailed evolution of specific developments is discussed hereinafter.

3.2. Route origins and dissolution chemistry

In 2012, Liu *et al.* first used oleylamine (OLA) and dodecanethiol (DT) mixed solvents to dissolve $CuCl_2$, $SnCl_4$, $ZnCl_2$ and Se to synthesize high-quality $Cu_2ZnSnSe_4$ NCs. However, they proposed that the Se solution was very stable in amines and thiols, while it could be dissolved in their mixtures through oxidation reactions.[67] In 2013, Bruchey *et al.* demonstrated that a binary solvent mixture of 1,2-ethylene glycol and 1,2-ethylenediamine at a volume ratio of 1 : 10 could rapidly dissolve V–VI chalcogenides (V = As, Sb, Bi; VI = S, Se, Te); the photograph of all nine V_2VI_3 semiconductors solutions are shown in Fig. 4a.[64] Subsequently, Bruchey *et al.*, using the solvent ratio configuration of EN/EDT, prepared Sb–Se precursor solution and Sn–Te precursor solution, achieving high crystallization Sb_2Se_3 and SnTe thin films in 2014.[68] In 2015, Brutchey also reported the application of $Sb_2Se_{3-x}S_x$ thin films by dissolving Sb_2O_3 and Se in a suitable ratio of EN/EDT solvent.[69] In addition, Lin *et al.* also used EN/EDT solvent (EN/EDT ratio = 1 : 10) to dissolve inorganic semiconductors (Cu_2S, Cu_2Se, In_2S_3, In_2Se_3, CdS, and SnSe) at room temperature and atmospheric pressure (Fig. 4b), and they also demonstrated that these ink materials can be easily processed into high-performance semiconducting thin films, such as Cu_2S and Cu_2Se.[70] The EN/EDT solution has strong solubility for metal sulfides, metal chlorides and metal oxides. Furthermore, the highest solubility for various solutes also differed slightly by adjusting the ratio of binary solvents. Additionally, EN/EDT can dissolve sulfide and selenide to obtain the corresponding precursor solution to prepare sulfide, selenide and telluride

Table 2 A selected summary of precursor ink formulations, heat treatments, and device performances for $Cu_2ZnSn(S,Se)_4$ solar cells using amine–thiol-based-solution-deposited absorbers. PCE is the total area unless otherwise stated

Year	Solar cell	Molecular ink	Dissolution condition	Heat treatments	Area [cm^2]	V_{OC} [mV]	J_{SC} [mA cm^{-2}]	FF [%]	PCE [%]	Institute	Ref.
2015	CZTSSe	Solution A: CuCl, $ZnCl_2$, and $SnCl_2$ into a mixture of hexylamine and propanethiol; solution B: Se powder and S flakes into a combination of hexylamine and propanethiol	N_2, glove box	Annealed (500 °C)	0.47	382	34.4	60.1	7.86[a]	PU	45
2015	CZTSSe	Cu, Zn, Sn, S, and Se of 1,2-ethanedithiol and 1,2-ethylenediamine	Stirring (70 °C)	Annealed (550 °C)	0.19	361	32.00	55.4	6.4	HENU	44
2015	CZTSSe	Cu_2O, ZnO, SnO into 2-methoxyethanol, 1,2-ethanedithiol, and ethanolamine	Stirring	Annealed (540 °C)	0.425	436	34.03	49.5	7.34[b]	CIAC	74
2017	CZTSSe	Cu, Ag, Zn, Sn, S, and Se powders were dissolved in a solvent mixture of 1,2-ethanedithiol and 1,2-ethylenediamine	Stirring (60 °C)	Annealed (480 °C)	0.21	448	35.19	65.66	10.36[b]	HENU	71
2018	CZTSSe	Cu, Zn, Sn, S, and Se of ethanolamine and cysteamine	Stirring	Annealed (330 °C + 575 °C)	0.25	420	30.8	62	8.1[b]	LU	72
2019	CZTSSe	Cu, Zn, Cd, Sn, S, and Se powders were dissolved in the mixture of 1,2-ethanedithiol and 1,2-ethylenediamine	Stirring	Annealed (550 °C)	0.21	386	29.36	57.26	6.49[b]	FZU	75
2020	CZTSSe	Cu, Zn, Sn, S, and Se of ethylenediamine and 1,2-ethanedithiol + stabilizing with GeO_2	N_2,glove box	Annealed (510 °C)	0.21	489.2	37.14	67.47	12.26[a,b]	HENU	73
2020	CZTSSe	Cu, Zn, Sn (or a mixture of Sn and In), Se, and S were mixed into 1,2-ethanedithiol and 1,2-ethylenediamine solution	Stirring	Annealed (550 °C)	0.21	393	32.12	56.96	7.19[b]	FZU	90
2021	CZTSSe	Cu, Zn, Sn, S, and Se of ethylenediamine and 1,2-ethanedithiol + stabilizer	Stirring (65 °C)	Annealed (550 °C)	0.21	480.3	37.87	69.00	12.54[a,b]	HENU	65
2021	CZTSSe	Cu, Zn, Sn, S, and Se of 1,2-ethanedithiol and 1,2-ethylenediamine + stabilizer	Stirring (70 °C)	Annealed (550 °C)	0.21	491	34.77	67.23	11.48[a,b]	HENU	76
2021	CZTSSe	Cu, Zn, Sn, S, and Se into the mixture of 1,2-ethanedithiol (EDT) and 1,2-ethylenediamine (EN) + Ga and Se into the mixture of EDT and EN + stabilizer	Stirring (70 °C)	Annealed (550 °C)	0.21	515	34.78	68.55	12.3[a,b]	HENU	78
2021	CZTSSe	Cu, Zn, Sn, S, and Se of 1,2-ethanedithiol and 1,2-ethylenediamine + stabilizer	Stirring (70 °C)	Annealed (550 °C)	0.21	495	37.07	66.26	12.16[a,b]	HENU	79
2021	CZTSSe	Cu, Zn, Sn, S, and Se of 1,2-ethanedithiol and 1,3-ethylenediamine + stabilizer	Stirring	Annealed (550 °C)	0.21	456	36.6	67.1	11.23[a,b]	HENU	80
2021	CZTSSe	Cu, Zn, Sn, S, and Se of 1,2-ethanedithiol and 1,4-ethylenediamine	Stirring	Annealed (550 °C)	0.21	496	36.64	67.89	12.34[a,b]	HENU	81
2022	CZTSSe	Cu, Zn, Sn, S, and Se of 1,2-ethanedithiol and 1,4-ethylenediamine	Stirring	Annealed (550 °C)	0.21	505	35.31	65.88	11.75[b]	HENU	91
2022	CZTSSe	Cu, Zn, Sn, S, and Se were dissolved in a mixed solvent of 1,2-ethanedithiol and 1,2-ethylenediamine + LiOH	Stirring	Annealed (550 °C)	0.21	459	31.98	65.94	9.68[b]	FZU	77
2022	CZTSSe	Cu, Zn, Sn, S, and Se were dissolved in a mixed solvent of 1,2-ethanedithiol and 1,2-ethylenediamine	Stirring (70 °C)	Annealed (300 °C + 550 °C)	0.21	463	35.65	62.47	10.24[a,b]	FZU	82

[a] Cells with ARC. [b] Active area.

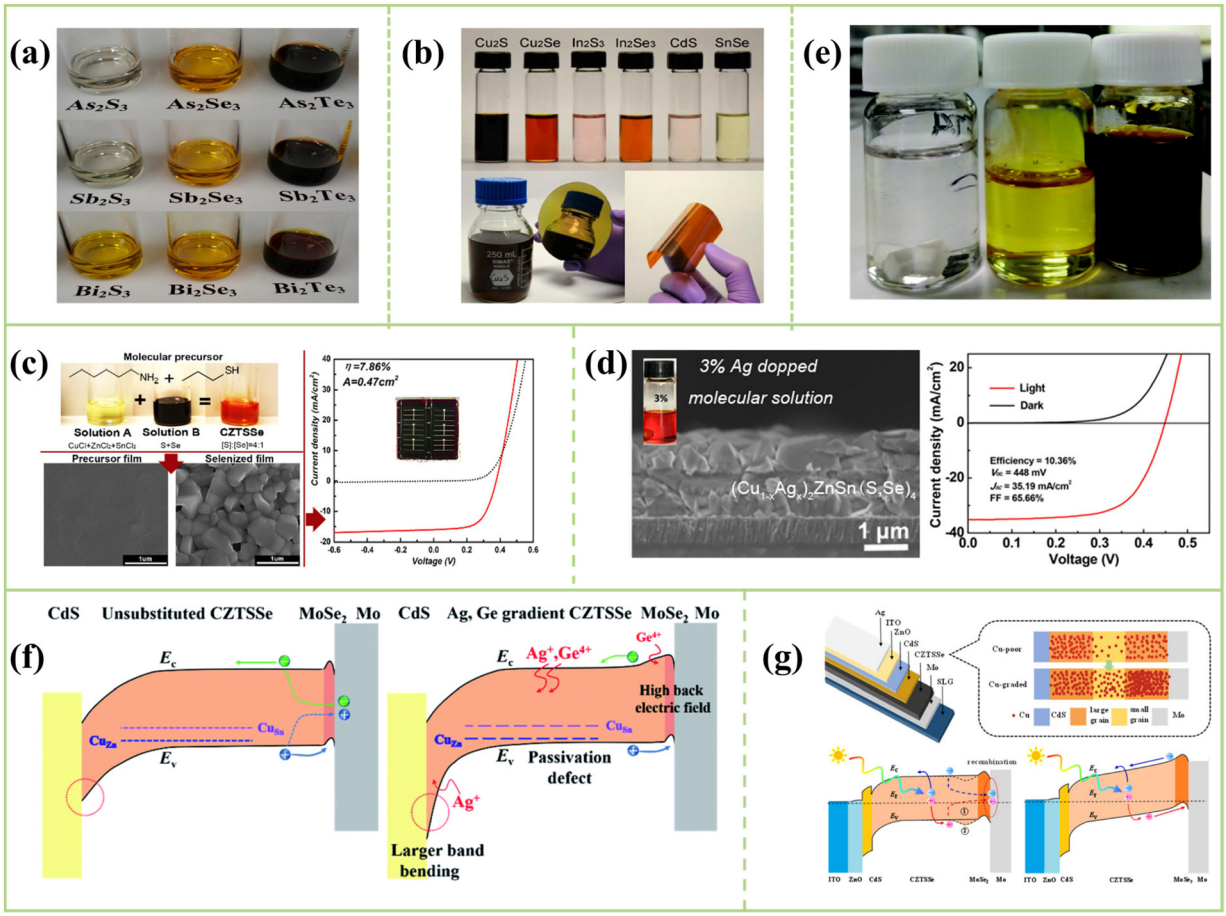

Fig. 4 (a) Photograph of all nine V_2VI_3 semiconductors in a 1 : 10 v/v 1,2-ethanedithiol/1,2-ethylenediamine solvent mixture.[64] Copyright © 2013, American Chemical Society. (b) Photograph of solubility of Cu_2S, Cu_2Se, In_2S_3, In_2Se_3, CdS, and SnSe in a binary mixed solvent of amine and thiol.[70] Copyright © 2015, American Chemical Society. (c) Photograph of the precursor solution, absorber layer morphology and *J*–*V* curves prepared by Agrawal.[45] Copyright © 2015, American Chemical Society. (d) Cross-section and *J*–*V* curves of 10.36% CZTSSe solar cells.[71] Copyright © 2017 American Chemical Society. (e) Left to right: 10 : 1 ETA/CA; precursor solution of Cu, Zn, Sn, S; precursor solution of Cu, Zn, Sn, and Se.[72] Copyright © 2020, Royal Society of Chemistry. (f) Schematic diagrams of the energy band structure of the unsubstituted and Ag, Ge dual-gradient CZTSSe thin-film solar cells.[73] (Left) shows the smaller band bending at the p–n junction, larger carrier recombination at the back contact and high concentration of deep-level defects within the bulk in traditional kesterite devices. (Right) presents the downshift of VBM *via* Ag substitution, the upshift of CBM through Ge substitution and the decreased concentration of deep-level defects within the bulk. Copyright © 2020, Royal Society of Chemistry. (g) Top of established carrier concentration gradient for bottom Cu-higher CZTSSe solar cells and traditional and ideal concentration gradient-mediated charge transport processes within CZTSSe solar cells. (bottom-left) shows the specific recombination routes between electrons and holes because of the inferior charge transport within the quasineutral region and generated EV notch at back contact for Cu-poor devices. (bottom-right) Enhanced driven force of electrons diffusion toward front contact.[65] Copyright © 2021 American Chemical Society.

thin films from the studies by Lin and Brutchey. Based on previous studies, the application of kesterite solar cells prepared by this system has achieved great progress.

3.3. PV applications for amine thiol-based routes

In 2015, Agrawal *et al.* applied EN/EDT mixed solvent to prepare CZTSSe thin film solar cells for the first time. They used the mixed solvent to obtain the CZTSSe precursor solution (Fig. 4c) by mixing solution A (CuCl, $ZnCl_2$, and $SnCl_2$ into a mixture of hexylamine and propanethiol) and solution B (Se powder and S flakes into a combination of hexylamine) under low-temperature annealing, achieving a full area PCE to 7.86%.[45] However, the precursor solution is composed of chloride by Agrawal, and atomic Cl as a heteroatom may seriously affect device performance. Therefore, Wu's group explored the solubility of Cu, Zn, Sn, Sn, S and Se powders in ethylenediamine and ethanedithiol for the first time, and they revealed that these low-cost elements can not only simultaneously dissolve but also form a homogeneous CZTSSe precursor solution in a short time, obtaining high crystallinity thin film with an efficiency of 6.4%.[44] In addition, Pan's group developed a new solution method by dissolving metal element, metal oxide and metal hydroxide in ethanedithiol/ethanolamine/ethylene glycol methyl ether for CZTSSe devices; this system can dissolve the precursor materials at room temperature faster than the previous solvent, and the efficiency is as

high as 7.34%.[74] Furthermore, Qi *et al.* dissolved elemental Cu, Ag, Zn, Zn, Sn, S and Se powders in a solvent mixture of 1,2-ethanedithiol and 1,2-ethylenediamine, and they found that adding a small amount of Ag^+ into the host lattice of CZTSSe films significantly improved the crystal growth of CZTSSe films, and the PCE of CAZTSSe solar cells increased from 7.39% to 10.36% (Fig. 4d).[71] However, the mechanism for CZTS precursors in amine thiol systems has not been elucidated in detail. Therefore, Malkov *et al.* studied the dissolution process of CZTS solar cells using an amine–thiol system in 2018. Fig. 4e shows the dissolution of metals in ethanolamine and mercaptoethylamine, mainly forming metal complexes with cysteamine, but sulfur, ethanolamine, oxygen and nitrogen could coordinate to the metal center, and the final fabricated device has an efficiency of 8.1%.[72] In 2020, Wu's group proposed an Ag, Ge double gradient absorbers structure, which achieves the down-shift of the valence band of the front-contact and the up-shift of the conduction band of the back-contact, improving the performance of CZTSSe devices and achieved an efficiency of 12.26% (Fig. 4f).[73] In recent years, Wu's group has made a lot of inspiring achievements in the preparation of CZTSSe thin film solar cells in the amine/thiol solvent system, and they achieved the highest efficiency of 12.54% using the local Cu component engineering (Fig. 4g).[65]

3.4. Extrinsic doping of amine thiol-based routes

3.4.1. Cationic equivalent substitution. The characteristics of the multielement of CZTSSe lead to numerous intrinsic defects. In recent years, researchers have aimed to reveal the defect formation mechanism and passivation strategies. For example, extensive theoretical and experimental studies by the group of Persson[83–85] and Carter[86–88] have shown that Na, Ca, Cd, Si, and Ge as alloying elements are expected to enhance the performance of CZTSSe devices. In 2017, Qi *et al.* dissolved silver elements in 1,2-ethylene glycol and 1,2-ethylenediamine solvents and obtained CAZTSSe (Ag/(Cu + Ag) = 3%) solar cells up to 10.36%, and they observed that the grain growth of the absorbers is significantly improved, which is beneficial to the improvement of the I–V characteristics of CZTSSe.[71] In 2019, Yan *et al.* prepared $Cu_2Zn_{1-x}Cd_xSn(S, Se)_4$ (x = 0.15%) solar cells by partially replacing Zn with Cd, and they believed that Cd is beneficial to the growth of grains and can effectively suppress Cu_{Zn} and Zn_{Cu} defects. When Cd/(Zn + Cd) = 8%, the optimal device efficiency is 6.49%. Fig. 5a shows the cross-sectional SEM image of flexible $Cu_2Zn_{1-x}Cd_xSn(S,Se)_4$ solar cells.[75] Recent studies have shown that the deep point defects of Sn_{Zn} and their defect clusters are also considered to be one of the important reasons limiting the PCE improvement of kesterite solar cells.[89] Moreover, Deng *et al.* proposed a strategy to incorporate Ge to reduce the Sn_{Zn} defect concentration and achieved a PCE of 11.48% CZTSSe solar cells, and the cross-sectional SEM images of reference (left) and 15 nm Ge samples (right) are shown in Fig. 5b and c.[76] Cheng's group also used Li doping to obtain a device efficiency of 9.68% in flexible CZTSSe solar cells (Fig. 5d).[77]

3.4.2. Cationic unequivalent substitution. In 2020, Cheng's group effectively passivated deep-level defects by replacing Sn^{4+} with In^{3+}, and the PCE was 7.19% when In/(Sn + In) = 9%, reducing interfacial recombination and band tails.[90] In 2021, Du *et al.* proposed that a Ga/(Ga + Zn + Sn) ratio of 5.0% effectively passivated Cu_{Zn} and Sn_{Zn} defects and achieved an impressive PCE of 12.3% (Fig. 5e).[78]

In addition to the above reports, Wu's group has developed strategies, such as alkali metal post-deposition treatment (PDT), supercritical carbon dioxide treatment, surface defect ordering and co-selenization, to improve device performance.[79–81,91] In addition, Cheng's group has also increased the efficiency of flexible CZTSSe solar cells to 10.24% using a pre-selenization process.[82]

According to the above beneficial optimization strategy, the highest efficiency of CZTSSe devices was 12.54% manufactured by an amine–thiol solvent. This efficiency is basically the same as that of other solvent systems. At present, the main problem is that absorbers can only obtain the double-layer structure (a large grain/fine grain) or the sandwich absorber structure (a large grain/fine grain/large grain) in the amine–thiol solvent system. According to reports, the reason for the fine grain layer structure is mainly due to the residual organic carbon impurities in the precursor films and the incomplete solvent volatilization in the amine–thiol mixed solvent. These organic carbon impurities seriously inhibit grain growth during high-temperature selenization, resulting in the formation of thicker carbon-rich grain layers and a layered structure in the CZTSSe absorbers. In addition, the fine grain layers lead to a relatively large number of grain boundaries in the absorbers, which increases the density of defect states and leads to the rapid recombination of photogenerated carriers. However, a new shunt path is created that adversely affects the R_{sh} and FF of the CZTSSe device. Therefore, it is necessary to further develop new and effective strategies, such as optimizing the selenization process and regulating the element ratio of the precursor solution, to eliminate the small grain layer structure, obtaining perfect crystallinity, such as DMF and DMSO, reducing the grain boundary and improving the grain size. These beneficial pathways further improve the performance of CZTSSe solar cells using amine–thiol.

4. Aprotic solvents

4.1. DMSO–Thiourea ($(CH_3)_2SO$)-$SC(NH_2)_2$

To avoid the use of toxic solvents, dimethyl sulfoxide (DMSO)-based processing acts as a promising deposition route for molecular-based precursor solutions. DMSO is an extremely soluble, inexpensive, and commercially available solvent, which is not only an aprotic, higher polar solvent but can also well dissolve metal salts.[92] Hilhouse *et al.* were the first to apply CZTSSe in DMSO. The DMSO solution method has the following advantages: (i) high polarity, good solubility for metal inorganic salts, and easy doping of materials; (ii) low toxicity, which is conducive to large-scale and commercial

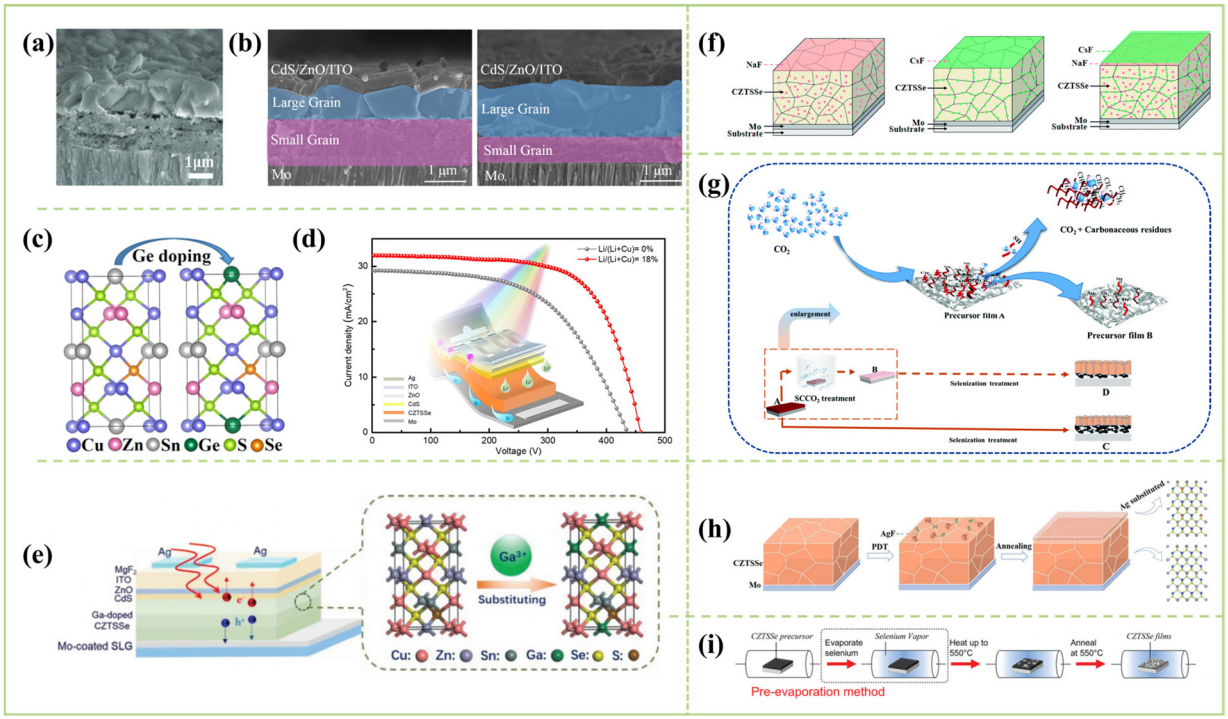

Fig. 5 (a) The cross-section SEM image of flexible $Cu_2Zn_{1-x}Cd_xSn(S,Se)_4$ solar Cells.[75] Copyright © 2019, WILEY-VCH Verlag GmbH & Co. KGaA. (b) The cross-sectional SEM images of reference (left) and 15 nm Ge samples (right).[76] Copyright © 2021, Elsevier. (c) Schematic of CZTGSSe solar cell with the model of doping Ge^{4+}: replacing Sn^{4+}.[76] Copyright © 2021, Elsevier. (d) Main structure diagram of the flexible CZTSSe solar cell and *J*–*V* curves.[77] Copyright © 2022, Elsevier. (e) Schematic structure of CZTGSSe solar cell and the model of doping Ga^{3+}: replacing Zn^{2+} and Sn^{4+}.[78] Copyright © 2021, Wiley-VCH GmbH. (f) Left–right: schematic diagrams of the alkali element distribution within the Na, Cs, and Na–Cs incorporated CZTSSe absorber; the pink and green dots represent Na and Cs atoms, respectively.[79] Copyright © 2021, Royal Society of Chemistry. (g) Schematic illustration of $SCCO_2$ treatment on CZTSSe film fabrication.[80] Copyright © 2020, Royal Society of Chemistry. (h) Schematic of typical operation procedures for the preparation of AgF-PDT CZTSSe absorber.[81] Copyright © 2022, Elsevier. (i) Schematic diagram of pre-evaporation selenization (PES) method.[82] Copyright © 2022, Wiley-VCH GmbH.

applications; (iii) thermal stability of the good solution, which is not easy to deteriorate; (iv) good volatility and less carbon residue, which is conducive to preparing high-quality large-sized crystalline thin films; and (v) moderate solvent viscosity, suitable for spin-coating thin films preparation. Currently, record PCEs of 13.0% (certified cell efficiencies) have been reported from DMSO molecular inks in 2021 (Table 3).[93,94]

4.1.1. PV applications for DMSO/TU-based routes. In 2011, an efficiency of 4.1% of the CZTSSe device was prepared using metal inorganic salts ($Cu(OAc)_2{\cdot}H_2O$, $SnCl_2$, $ZnCl_2$) and organic ligand thiourea ($SC(NH_2)_2$, Tu) in DMSO by Hilhouse's group for the first time.[93] Based on this research, Hilhouse's group improved the preparation process of the precursor solution in 2014, increased the grain size, and reached an efficiency of 8.32%. Fig. 6(a) shows photos of the solution before and after improvement. They believed this color difference was due to the redox reaction.[95] Furthermore, Haass *et al.* adopted a similar method using a three-stage annealing process, improving the grain size and morphology of the films, and the efficiency reached 11.2% (Fig. 6b).[94] In the same year, Hillhouse *et al.* obtained an efficiency of 11.8% CZTSSe device (Fig. 6c) by doping lithium chloride in the molecular precursor solution. This efficiency was the highest CZTSSe solar cell by non-hydrazine solution treatment at that time. They controlled the defect chemistry by solution doping to further improve the efficiency of CZTSSe solar cells from a new window perspective, playing an important role in high-efficiency kesterite photovoltaics.[96] Although the cross-section of the device above comprises large particles on the top layer and very narrow fine particles on the bottom layer, there are obvious microscopic pores and more grain boundaries, which limit the device performance in the DMSO system.[97] In 2020, Xin's team used $SnCl_4$ and $SnCl_2$ $2H_2O$ as tin precursors to study the effect of the tin oxidation state on the performance of kesterite solar cells (Fig. 6d and e), and they discovered that the combination of Sn^{4+} and DMSO promoted the direct formation of the CZTS phase in the precursor film, which is directly converted to CZTSSe during the selenization process with an efficiency of 12.4%.[98] In 2021, based on the DMSO precursor solution method, Xin's team also effectively improved the quality of the CZTSSe absorbers by regulating the chemical reaction in the DMSO solution, and the PCE was as high as 12.5%.[99] In the same year, they achieved a certification efficiency of 13.0% through a 10% Ag substitution strategy.[24,100] In 2022, Meng's group proposed a new effective strategy to simultaneously

Table 3 A selected summary of precursor ink formulations, heat treatments, and device performances for $Cu_2ZnSn(S,Se)_4$ solar cells using DMSO and DMF-based solution-deposited absorbers. PCE is the total area unless otherwise stated

Year	Solar cell	Molecular ink	Dissolution condition	Heat treatments	Area [cm^2]	V_{OC} [mV]	J_{SC} [mA cm^{-2}]	FF [%]	PCE [%]	Institute	Ref.
DMSO molecular inks											
2011	CZTSSe	$Cu(CH_3COO)_2$ H_2O, $ZnCl_2$, $SnCl_2{\cdot}2H_2O$, and thiourea into dimethyl sulfoxide	Stirring	Annealed (580 °C) + selenized (500 °C)	0.47	400	24.9	41.2	4.1	UW	93
2014	CZTSSe	$Cu(CH_3COO)_2$ H_2O, $ZnCl_2$, $SnCl_2{\cdot}2H_2O$, and thiourea into dimethyl sulfoxide	Stirring	Annealed (540 °C) + selenized (540 °C)	0.43	443	31.2	60.2	8.32[b]	UW	95
2015	CZTSSe	$CuCl_2$, $SnCl_2{\cdot}2H_2O$, $ZnCl_2$, Tu, NaCl into DMSO	Stirring	Annealed (300, 500, 550 °C)	0.30	479	36.5	63.8	11.2	EMPA	94
2015	CZTSSe	$Cu(CH_3COO)_2$ H_2O,$SnCl_2$ $2H_2O$,$ZnCl_2$, TU,LiF into DMSO	Stirring	Annealed (540 °C)	0.10	449	38.8	68.1	11.8[b]	UW	96
2018	CZTSSe	CuCl, $SnCl_2{\cdot}2H_2O$, $ZnCl_2$,NaCl into DMSO + Tu	Stirring	Selenized	0.19	463	33.4	65.5	10.1[b]	CIAC	102
2018	CZTSSe	Tu,$SnCl_2{\cdot}2H_2O$, $ZnCl_2$, $CuCl_2{\cdot}2H_2O$ and LiCl dissolved in DMSO	Stirring	Annealed (300, 500, 550 °C)	0.28	531	33.7	64.8	11.6	EMPA	103
2018	CZTSSe	$Cu(CH_3COO)_2{\cdot}H_2O$, $Zn(CH_3COO)_2{\cdot}2H_2O$, $SnCl_2$ and CH_4N_2S into dimethyl sulfoxide + H_2O + $AgNO_3$	Stirring	Selenization (530 °C)	0.11	477	35.7	61.4	10.3[b]	LICP CAS	104
2020	CZTSSe	CuCl-Tu, $SnCl_4$-DMSO-$Zn(OAc)_2$ into DMSO	N_2, glove box	Selenised (550 °C)	0.11	522	33.32	71.5	12.4	NJUPT	98
2021	CZTSSe	CuCl-Tu, $SnCl_4$-DMSO-$Zn(OAc)_2$ into DMSO	N_2, glove box	Selenised (550 °C)	0.11	499	36.4	68.0	12.4	NJUPT	98
2021	CZTSSe	$AgNO_3$-CuCl-Tu, $SnCl_4$-DMSO-$Zn(OAc)_2$ into DMSO	N_2, glove box	Selenised (550 °C)	0.11	540	32.1	72.3	12.5	NJUPT	99
2021	CZTSSe	$AgNO_3$-CuCl-Tu, $SnCl_4$-DMSO-$Zn(OAc)_2$ into DMSO	N_2, glove box	Selenised (550 °C)	0.11	529.4	33.58	72.9	13.0[a,b]	NJUPT	100
2022	CZTSSe	CuCl, $SnCl_2{\cdot}2H_2O$, $ZnCl_2$, and $SC(NH_2)_2$ were added to DMSO	Stirring	Selenised (550 °C)	0.19	405.67	36.86	57.78	8.64[b]	JLU	105
2022	CZTSSe	CuCl, $ZnCl_2$, $SnCl_2{\cdot}2H_2O$, and CH_4N_2S into DMSO	Stirring	Selenised (560 °C)	0.11	481	35.10	63.09	10.65[b]	NWNU	106
2022	CZTSSe	Thiourea was added into vial 1 containing 15 mL DMSO; then, AgCl and CuCl were added into vial 1 and stirred till completely dissolved. 15 mL DMSO was injected into vial 2 containing $SnCl_4$ under stirring. Then, $Zn(Ac)_2$ was added into the $SnCl_4$–DMSO suspension until dissolved completely	Stirring	Selenized (350 °C + 545 °C)	0.26	547.2	34.3	0.70	13.14	IOP, CAS	101
DMF molecular inks											
2015	CZTS	$Cu(CH_3COO)_2{\cdot}H_2O$, $Zn(CH_3COO)_2{\cdot}2H_2O$, $SnCl_2{\cdot}2H_2O$, Tu in DMF	Stirring (50 °C)	Sulfurized (580 °C, sulfur/N_2 atmosphere)	0.45	606	14.27	55.2	4.77	CSU	111
2019	CZTSSe	$Cu(CH_3COO)_2{\cdot}H_2O$, $SnCl_2{\cdot}2H_2O$, $ZnCl_2$, Tu in DMF	Stirring	Annealed (550 °C)	0.19	417	36.70	52.27	8.01[b]	JLU	114
2019	CZGTS	CuCl, $ZnCl_2$, and $GeCl_4$, DMF-TU	N_2, glove box	Annealed (540 °C)	0.105	583	33.60	55.9	11.0[b,c]	UW	115
2020	CZTSSe	$Cu(CH_3COO)_2H_2O$, $SnCl_2{\cdot}2H_2O$, $(CH_3COO)_2$ $Zn{\cdot}2H_2O$, and H_2NCSNH_2 in DMF solutions	N_2, glove box	Selenized (350 °C + 570 °C)	0.19	477	36.34	67.09	11.63[b]	NKU	116
2021	CZTSSe	CuCl, $SnCl_4$, $Zn(OAc)_2$, Tu in DMF	N_2, glove box	Ar, Annealed (350 °C + 540 °C)	0.105	491	33.20	70.6	11.5[b]	NJUPT	112
2022	CZTSSe	$Cu(OAC)_2{\cdot}H_2O$, $SnCl_2{\cdot}2H_2O$, $ZnCl_2$,Tu in DMF	Stirring	Annealed (550 °C)	0.21	501	35.36	66.4	11.76[b,c]	XCU	113
2022	CZTSSe	$Cu(CH_3COO)_2H_2O$, $SnCl_2{\cdot}2H_2O$, $(CH_3COO)_2Zn{\cdot}2H_2O$, and H_2NCSNH_2 in DMF solutions	N_2, glove box	Selenized (350 °C + 570 °C)	0.19	484.75	37.37	67.69	12.25[b]	NKU	117
DMSO/DMF molecular inks											
2019	CZTSSe	$Cu(NO_3)_2{\cdot}3H_2O$,$Zn(CH_3COO)_2{\cdot}2H_2O$,$SnCl_2{\cdot}2H_2O$, and $SC(NH_2)_2$ into DMSO	Stirring	Annealed (560 °C)	0.36	460	32.2	58.2	8.6	SYSU	108 and 109
2022	CZTSSe	$Cu(CH_3COO)_2{\cdot}H_2O$, $SnCl_2{\cdot}2H_2O$, $ZnCl_2$, and CH_4N_2S into DMF/DMSO binary solvents	Stirring	Selenized (530 °C)	0.20	493.5	33.89	73.30	12.26[b]	HBU	110

[a] Certified cell efficiencies. [b] Active area. [c] Cells with ARC.

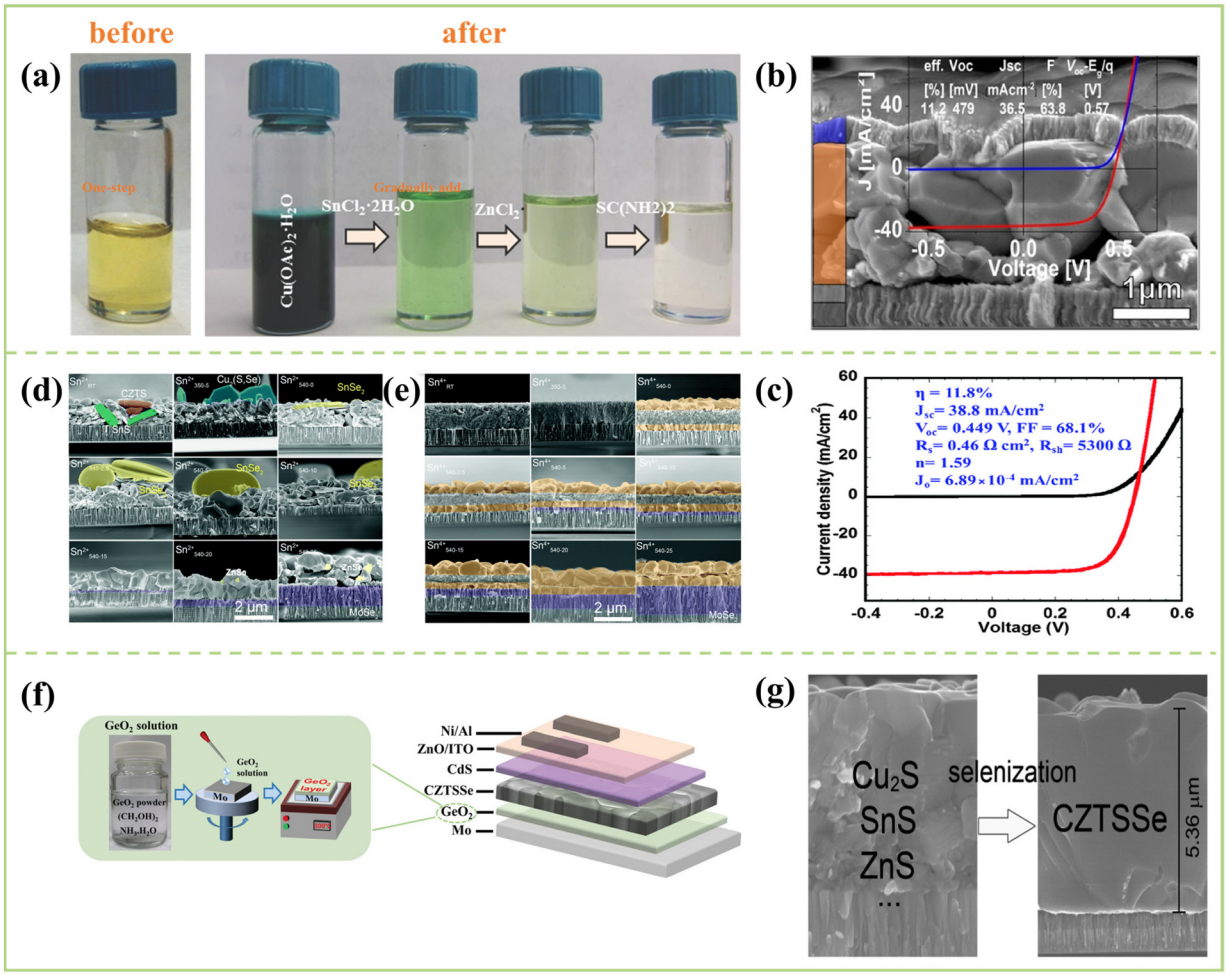

Fig. 6 (a) Photograph of the solution made by dissolving all precursors simultaneously in solvent (one step) and solutions in each step of the precursor solution preparation (gradually added).[95] Copyright © 2014, WILEY-VCH Verlag GmbH & Co. KGaA. (b) SEM cross-section image with an efficiency of 11.2% and its *J*–*V* characterization.[94] Copyright © 2015, WILEY-VCH Verlag GmbH & Co. KGaA. (c) *J*–*V* characteristics of the champion CZTSSe solar cell measured in the dark and under AM 1.5 simulated sunlight.[96] Copyright © 2015, Royal Society of Chemistry. (d) Cross-sectional SEM images of Sn^{2+}[98] and (e) Sn^{4+} films at various stages of the selenization.[98] Copyright © 2021, Royal Society of Chemistry. (f) Schematic structure of the $Cu_2ZnSn(S,Se)_4$ device with GeO_2 layer derived from spin-coating GeO_2 precursor solutions.[101] Copyright © 2022, Wiley-VCH GmbH. (g) Cross-sectional SEM images for preparing Cu_2S/SnS/ZnS mixed precursor thin films.[102] Copyright © 2018, American Chemical Society.

modulate the CZTSSe rear interface and suppressed the defects of the CZTSSe absorbers by introducing a thin germanium dioxide layer on the Mo substrate (Fig. 6f). The champion device has a V_{OC} of 547 mV and a PCE of up to 13.14% (pore area: 0.25667 cm^2).[101]

4.1.2. Extrinsic doping of DMSO/TU-based routes. An absorber with a large grain size is an ideal material for high-performance CZTSSe solar cells. However, most CZTSSe solar cells fabricated by DMSO in the early stage have a double layer structure with large particles in the upper layer and fine particles in the bottom layers. Therefore, Pan's group developed a phase separation strategy to promote the crystal growth of CZTSSe thin films by choosing zinc chloride, tin chloride, cuprous chloride (instead of cupric chloride) and thiourea as materials to prepare Cu_2S/SnS/ZnS mixed precursor thin films, and the efficiency of the large grain CZTSSe thin films was over 10% (Fig. 6g).[102] Cabas-Vidani *et al.* used lithium alloying to improve the efficiency to 11.6%.[103] In addition, Zhao *et al.* optimized the process of the precursor solution by adding an appropriate amount of water to the DMSO precursor solution.[104] Strategies, such as the valence state of tin, the different oxidation states of copper salts, and the regulation of element ratios, have also been applied to the absorbers by DMSO solvents.[105–107] Furthermore, Lin *et al.* added DMF to the DMSO-based CZTS precursor solution to improve the wettability between the precursor and the Mo substrate, thereby improving the quality of CZTSSe absorbers; however, the highest conversion efficiency reached only 8.6% when the proportion of additive DMF is 20%.[108,109] Fortunately, Sun *et al.* obtained more than 12% high-efficiency CZTSSe solar cells through the binary solvent engineering of DMF/DMSO in precursor solution in 2022.[110]

4.2. DMF–Thiourea ($(CH_3)_2NC(O)H$)-$SC(NH_2)_2$

4.2.1. DMF-Tu solvent system. To obtain high-quality kesterite absorbers and achieve higher efficiency, the selection of the solvent is extremely important. *N*,*N*-dimethylformamide (DMF) is a common solvent in many fields. However, it has a high solubility for metal sources (metal salts or oxides) and sulfur sources (such as sulfur, thiourea or thioacetamide). Its chemical properties are extremely stable and volatile. DMF is not only an attractive solvent for CZTS precursors but also accurately controls the composition of CZTSSe precursors to improve the performance of the device.[111,112] Because of its similar performance to DMSO, it can also achieve similar efficiency to DMSO. However, there are relatively few studies on CZTS absorbers by DMF compared with DMSO. Amazingly, a record PCE of 11.76% (cells with ARC) was reported from DMF-based molecular inks in 2022 (Table 3).[113] The reported efficiency of CZTSSe devices prepared by the DMF solution method is much lower than that of other solution methods, which indicates that there still is a great possibility of improving efficiency by exploring optimal strategic conditions to achieve the commercial production of CZTSSe solar cells.

4.2.2. Recent developments. In recent years, DMF has achieved great success in achieving high-efficiency CZTSSe solar cells. In early 2015, Liu *et al.* prepared CZTS thin films using a DMF solvent system for the first time and obtained only 4.77% PCE of the device. The photograph of the precursor solution and the morphology of the absorbers are shown in Fig. 7a.[111] Subsequently, Luan *et al.* improved the efficiency of CZTSSe solar cells to 8.01% by optimizing the proportion of cations, and the technological process for CZTS precursor solution are shown in Fig. 7b.[114] In addition, the optimization strategies of Na doping and Ge doping have also achieved satisfactory success with the best efficiency of 5.68% and 11%, respectively.[115] The above preliminary studies mainly focus on the improvement of device performance. However, in recent reports, Xin's team explained the solution chemistry and the reaction path from solution to absorbers using DMF. They found that the precursor films from Sn4+ and Cu+ avoided the formation of secondary phases (ZnS and SnS) during the pre-annealing process. In addition, Xin's team also found that $SnCl_4$ reacted with DMF to form complex $Sn(DMF)_2Cl_4$, while CuCl and $Zn(OAc)_2$ formed complexes with Tu, forming a precursor film of amorphous kesterite (CZTS) structure. However, its selenization process has a direct substitution reaction pathway and bidirectional top-down and bottom-up grain growth, resulting in a double large grain layer CZTSSe absorber structure (Fig. 7c). Eventually, the CZTSSe champion device reached 11.5% with an open circuit voltage of 0.491 V and a fill factor of 70.6%.[112] However, the absorbers obtained by Xin *et al.* are double large-grain layers, which may limit the further improvement of device performance. In addition, previous studies have also proved that if the absorber layer has a double- or triple-layer structure, it leads to a sharp increase in the grain boundaries of the absorbers, resulting in many recombination centers, which seriously affect the device efficiency. To solve the delamination phenomenon in the absorbers, in 2022, Zheng *et al.* used $Cu(CH_3COO)_2{\cdot}H_2O$, $SnCl_2$, $ZnCl_2$, and thiourea (TU) as precursor materials in the DMF solution system, utilizing the synergistic effect of the redox process of Sn^{2+} and Cu^{2+} and the pre-annealing temperature. The large-grain spanning monolayer was achieved for the first time, which improved the R_{sh} and R_{ct} of CZTSSe devices with an efficiency of up to 11.76%.[113] Additionally, Guo *et al.* used Se&LiF co-selenization process [116]and band-gap-graded [117]to achieved high efficiency CZTSSe solar cells of 11.63% and 12.25%, respectively.

Thus far, the highest efficiency of CZTSSe devices has been fabricated by DMSO solvent (13.0%, certified by NREL). However, the high-efficiency CZTSSe devices prepared by aprotic solvents (including DMSO and DMF) usually have a double layer or trilayer structure, introducing numerous grain boundaries, which are known to be detrimental to the carrier collection efficiency and device performance of CZTSSe solar cells. Therefore, the single large grain absorption layer by further regulating the grain growth process is beneficial to device performance. In addition, the metal-thiourea complexes and dispersed colloids formed in this system are easy to precipitate owing to the lack of strong solute–solvent interaction, resulting in instability of the prepared precursor solution. How to improve the stability of precursor solutions is also the key to high-efficiency devices. Furthermore, the CZTSSe thin films prepared by DMSO/DMF solvent do not use additional alkali metal doping and post-treatment, while many alkali metal element doping strategies reported in the literature can significantly improve the electrical properties of CZTSSe solar cells. Therefore, the development of alkali metal doping and post-treatment in DMSO/DMF solvents will further break through the current efficiency bottleneck.

5. Ethylene glycol methyl ether-based precursor solution method (EGME)

5.1. Route origins and dissolution chemistry

EGME, also known as ethylene glycol methyl ether, has been reported in the literature related to the thiol–amine system used to adjust the viscosity of the solution. In 2007, Tanaka *et al.* reported the CZTS precursor film by applying a sol–gel vulcanization method using ethylene glycol methyl ether as solvent and monoethanolamine (MEA) as a stabilizer, which is a very simple and inexpensive method for the preparation of CZTS thin films.[118] However, there are a couple of problems with this method while applying CZTSSe solar cells. On the one hand, the CZTS films showed low transparence in the infrared (IR) region; on the other hand, the CZTSSe absorbers contained small particles and voids.

Subsequently, Tanaka *et al.* reduced the pores of the CZTS films and increased the transmittance in the infrared region through a pre-annealing process in air, which promoted the

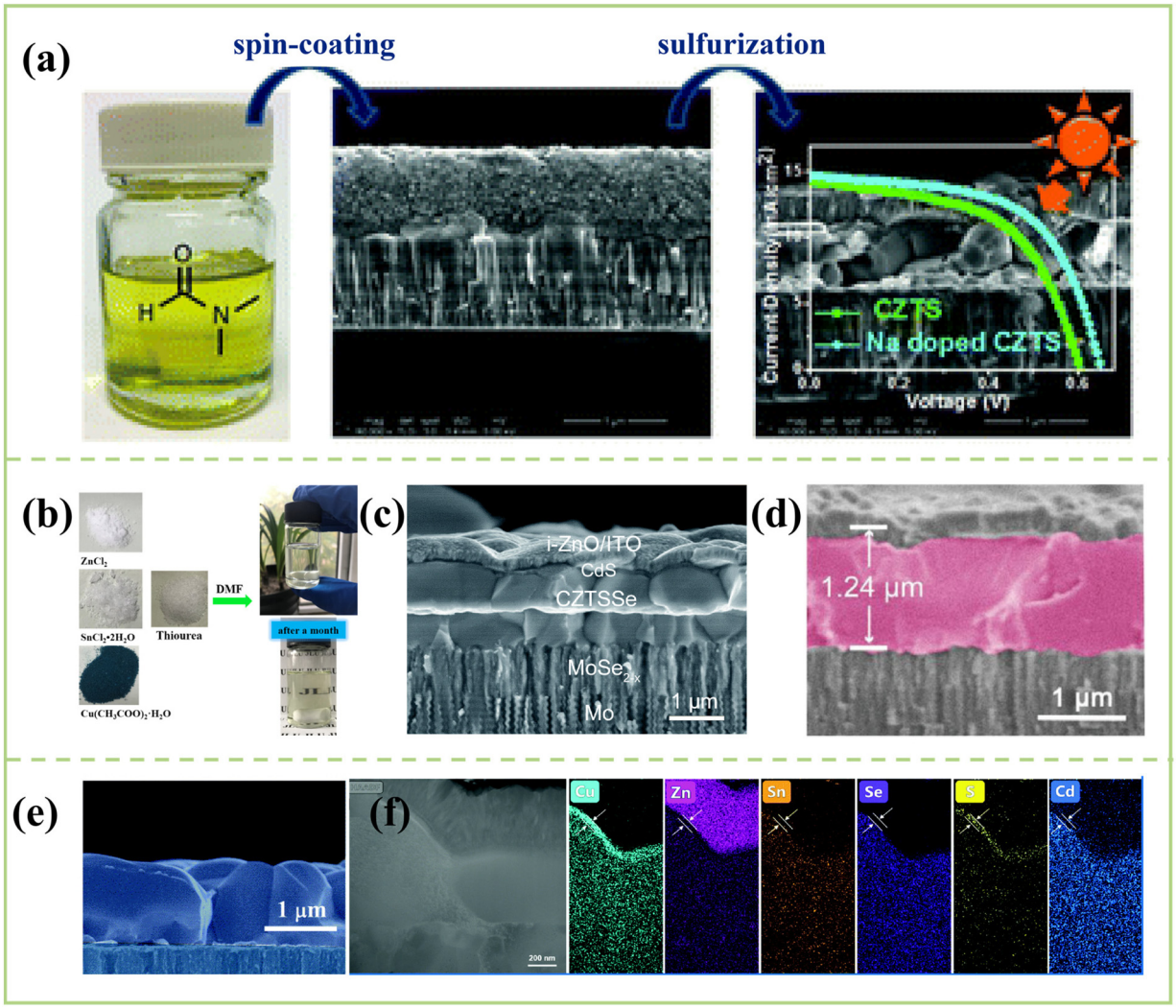

Fig. 7 (a) Photograph of the precursor solution and the morphology of the absorbers.[111] Copyright © 2015, Royal Society of Chemistry. (b) The technological process for the preparation of CZTS precursor solution with DMF as the solvent.[114] Copyright © 2019, Elsevier. (c) Cross-sectional SEM image of the CZTSSe solar cell with a PCE of 11.5%.[112] Copyright © 2021, Royal Society of Chemistry. (d) Cross-sectional images of the CZTSSe solar cell with a PCE of 11.76%.[113] Copyright © 2022, Wiley-VCH GmbH. (e) The cross-sectional SEM images of Se&LiF co-selenization processed samples.[116] Copyright © 2020, Royal Society of Chemistry. (f) The cross-section TEM morphologies and elemental mappings of the Se&LiF co-selenization processed CZTSSe devices.[117] Copyright © 2022, Royal Society of Chemistry.

development of high-efficiency CZTSSe solar cells by ethylene glycol methyl ether solution method.[119] Currently, a record PCE of 12.18% (certified cell efficiencies) has been reported from EGME molecular inks in 2021 (Table 4).[120]

5.2. PV applications for ethylene glycol methyl ether-based precursor solution routes

Tanaka *et al.* proposed and developed an ethylene glycol methyl ether solvent for CZTSSe solar cells. In 2009, Tanaka's team developed CZTS solar cells through sol–gel solutions of two concentrations of metal ions for the first time, but the efficiency was only 1.01%.[121] In the same year, Moritake *et al.* significantly improved V_{oc} by optimizing the deposition time of the CdS buffer layer, increasing the efficiency to 1.61%.[122] In 2011, Tanaka *et al.* obtained the highest efficiency of 2.03% for CZTS thin films by optimizing the composition ratio of Cu/(Zn + Sn) in the precursor solution.[123] Furthermore, Maeda *et al.* optimized the hydrogen sulfide concentration in the sulfurization process, and the highest CZTS solar cell efficiency was improved to 2.23%.[124] In 2011, Ilari *et al.* further improved the spin coating method of Tanaka *et al.* and achieved a selenide CZTSe absorbers with a grain size range of 1–2 μm and a uniform composition by optimizing the metal ratio in the precursor solution, thereby achieving an efficiency of 2.76%.[125] In 2013, Su *et al.* through Na-doped Cu_2ZnSnS_4 (CZTS) solar cells obtained an efficiency of up to 5.10%.[126] Subsequently, Su *et al.* also increased the efficiency to 5.7% by applying a low-pressure (0.04 MPa) vulcanization method.[127] In 2015, Zeng *et al.* improved the efficiency of CZTSSe devices to 8.08% by optimizing the selenization temperature, selenization time

Table 4 A selected summary of precursor ink formulations, heat treatments, and device performances for $Cu_2ZnSn(S,Se)_4$ solar cells using ethylene glycol methyl ether-based precursor solution method (EGME)-deposited absorbers. PCE is the total area unless otherwise stated

Year	Solar cell	Molecular ink	Dissolution condition	Heat treatments	Area [cm^2]	V_{OC} [mV]	J_{SC} [$mAcm^{-2}$]	FF [%]	PCE [%]	Institute	Ref.
2009	CZTS	$Cu(CH_3COO)_2{\cdot}H_2O$, $Zn(CH_3COO)_2{\cdot}2H_2O$, $SnCl_2{\cdot}2H_2O$ in 2-methoxyethanol and monoethanolamine	Stirring (45 °C–60 °C)	Annealed (300 + 500 °C)	0.15	390	7.81	33	1.01	NUT	121
2009	CZTS	$Cu(CH_3COO)_2{\cdot}H_2O$, $Zn(CH_3COO)_2{\cdot}2H_2O$, $SnCl_2{\cdot}2H_2O$ in 2-methoxyethanol (0.35M-ammonium acetate and DI water + 1.75M-monoethanolamine)	Stirring (45 °C)	Annealed (300 °C + 500 °C)	0.15	554	6.7	43.4	1.61[a]	NUT	122
2011	CZTS	$Cu(CH_3COO)_2{\cdot}H_2O$, $Zn(CH_3COO)_2{\cdot}2H_2O$, $SnCl_2{\cdot}2H_2O$ in 2-methoxyethanol (0.35M-ammonium acetate and DI water + 1.75M-monoethanolamine)	Stirring (45 °C)	Annealed (500 °C)	0.12	575	9.69	36.4	2.03	NUT	123
2011	CZTS	$Cu(CH_3COO)_2{\cdot}H_2O$, $Zn(CH_3COO)_2{\cdot}2H_2O$, $SnCl_2{\cdot}2H_2O$ in 2-methoxyethanol	Stirring (45 °C)	Annealed (500 °C)	0.12	529	10.2	41.6	2.23[a]	NUT	124
2012	CZTSe	$Cu(CH_3COO)_2{\cdot}H_2O$, $Zn(CH_3COO)_2{\cdot}2H_2O$, $SnCl_2{\cdot}2H_2O$ in 2-methoxyethanol and monoethanolamine	Stirring (50 °C)	Annealed (560 °C)	0.09	381	15.8	42.1	2.76[a]	EMPA	125
2014	CZTS	$Cu(CH_3COO)_2{\cdot}H_2O$, $Zn(CH_3COO)_2{\cdot}2H_2O$, $SnCl_2{\cdot}2H_2O$ and $SC(NH_2)_2$ were dissolved in 2-methoxyethanol	Stirring (50 °C)	Annealed (560 °C)	0.25	610	14.62	56	5.1	CSU	126
2014	CZTS	$Cu(CH_3COO)_2{\cdot}H_2O$, $Zn(CH_3COO)_2{\cdot}2H_2O$, $SnCl_2{\cdot}2H_2O$ and $SC(NH_2)_2$ in 2-methoxyethanol and monoethanolamine	Stirring (50 °C)	Sulfurization (580 °C)	0.25	664	14.8	58	5.7	CSU	127
2015	CZTSSe	$Cu(CH_3COO)_2{\cdot}H_2O$, $Zn(CH_3COO)_2{\cdot}2H_2O$, $SnCl_2{\cdot}2H_2O$ and excess SC $(NH_2)_2$ into 2-methoxyethanol + triethanolamine	Stirring (50 °C)	Annealed (500 °C–580 °C)	0.45	487	32.78	51	8.08[a]	CSU	128
2015	CZTS	$Cu(CH_3COO)_2{\cdot}H_2O$, $Zn(CH_3COO)_2{\cdot}2H_2O$, $SnCl_2{\cdot}2H_2O$, $SC(NH_2)_2$ and Cd $(CH_3\ COO)_2{\cdot}xH_2O$(Cd doping) in 2-methoxyethanol	Stirring (50 °C)	Annealed (250 °C + 580 °C)	0.25	581	24.1	66	9.82[a]	NTU	129
2015	CZTSSe	$CuCl_2$, $ZnCl_2$, $SnCl_2$ in 2-methoxyethanol + TU + $SbCl_3$(Sb doping)	Stirring	Annealed (260 °C + 520 °C)	0.12	464.4	30.6	57.8	8.2[a]	NTU	134
2016	CZTSSe	$Cu(OAc)_2{\cdot}H_2O$ into MeOH and 2-ME + $SnCl_2{\cdot}2H_2O$ + $Zn(OAc)_2{\cdot}2H_2O$ + TU + KOH(K doping)	Stirring	Annealed (560 °C)	0.12	446	32.22	55.97	8.04	CNSI	135
2016	CZTSSe	$CuCl_2$, $ZnCl_2$, $SnCl_2$ in EGME + TU in EGME	Stirring	Sulfurised (540 °C); selenised (520 °C)	0.141	450	36.5	61.9	10.1[a,c]	NCKU	130
2018	CZTS	$Cu(CH_3COO)_2{\cdot}H_2O$, $Zn(CH_3COO)_2{\cdot}2H_2O$, $SnCl_2{\cdot}2H_2O$, $SC(NH_2)_2$ in 2-methoxyethanol(Ag + Cd incorporation)	Stirring (50 °C)	Annealed (600 °C)	0.16	650	25	66.2	10.8 [a]	NTU	18
2018	CZTSSe	$CuCl_2$, $ZnCl_2$, $SnCl_2$ in EGME + TU in EGME	Stirring	Annealed(540 °C + 520 °C)	0.141	578	30.5	63	11.1[a]	NCKU	131
2020	CZTSSe	$Cu(CH_3COO)_2{\cdot}H_2O$, $ZnCl_2$, $SnCl_2{\cdot}2H_2O$ and thiourea into 2-methoxyethanol	Stirring (60 °C)	Annealed (550 °C)	0.2283	465.1	39.33	66.51	12.18[b,c]	CSU	120
2020	CZTS	$Cu(CH_3COO)_2{\cdot}H_2O$, $Zn(CH_3COO)_2{\cdot}2H_2O$ + $Cd(CH_3COO)_2{\cdot}xH_2O$, $SnCl_2{\cdot}2H_2O$, and $SC(NH_2)_2$ into 2-methoxyethanol	Stirring (60 °C)	Sulfurization (200 °C + 580 °C)	0.16	640	27.8	71	12.6[a]	CSU	132
2020	CZTS	$Cu(CH_3COO)_2{\cdot}H_2O$), $(Zn(CH_3COO)_2{\cdot}2H_2O$, $SnCl_2{\cdot}2H_2O$, thiourea in 2-methoxyethano + $AgNO_3$ and KCl	Stirring (50 °C)	Annealed (600 °C)	0.15	670	21.5	57.22	8.24[a]	NTU	137
2020	CZTS	$CuCl_2{\cdot}2H_2O$, $ZnCl_2$, $SnCl_2{\cdot}2H_2O$, and thiourea in 2-methoxyethanol with ethanolamine and triethanolamine + $MnCl_2$ $5H_2O$	Stirring (50 °C)	Annealed (560 °C)	0.15	471	31.7	58.57	8.74[a]	NTU	138
2021	CZTSSe	CuCl, $Zn(CH_3COO)_2{\cdot}2H_2O$, $SnCl_4{\cdot}5H_2O$, and $SC(NH_2)_2$ and Cu $(CH_3COO)_2{\cdot}H_2O$, $ZnCl_2$, $SnCl_2{\cdot}2H_2O$, and $SC(NH_2)_2$ into 2-methoxyethanol	Stirring (60 °C)	Annealed (555 °C)	0.135	507	33.97	65.36	11.1[a]	CSU	34
2022	CZTSSe	Zn $(CH_3COO)_2{\cdot}2H_2O$, CuCl, $SnCl_4{\cdot}5H_2O$ and CH_4N_2S in 2-methoxyethanol	Stirring (60 °C)	Selenized (565 °C)	0.135	505	39.43	61.45	12.07[a]	CSU	133
2022	CZTSSe	Zn $(CH_3COO)_2{\cdot}2H_2O$, CuCl, $SnCl_4{\cdot}5H_2O$ and CH_4N_2S in 2-methoxyethanol + AgCl in DMSO + $TiCl_4$ added into ethanol	Stirring (60 °C)	Annealed (555 °C)	0.135	530	37.49	64.04	12.73[a]	CSU	139
2022	CZTSSe	$ZnCl_2$, $SnCl_2{\cdot}2H_2O$, H_2O, $Cu(CH_3COO)_2{\cdot}H_2O$, and TU in 2-methoxyethanol	Stirring (60 °C)	Selenized (550 °C)	0.2402	494.1	36.22	67.46	12.07	CSU	140
2022	CZTSSe	CuCl, $Zn(CH_3COO)_2$ $2H_2O$, $SnCl_4$ $5H_2O$, AgCl, and $SC(NH_2)_2$ and Cu $(CH_3COO)_2$ H_2O, $ZnCl_2$, $SnCl_2{\cdot}2H_2O$, AgCl, and $SC(NH_2)_2$ into 2-methoxyethanol, respectively, the final precursor solution was obtained by mixing the two solutions in a 1 : 1 ratio	Stirring (60 °C)	Selenized (550 °C)	0.21	505.5	39.3	64.8	12.87	HENU	141

[a] Active area. [b] Cells with ARC. [c] Certified cell efficiencies.

and metal composition.[128] In the same year, they prepared a high-efficiency CZTS solar cell by the cation substitution (Cd substitution) with the best efficiency of 9.82%.[129] Moreover, Shih-Hsiung Wu *et al.* first dissolved the chloride salts of Cu, Zn, and Sn in ethylene glycol methyl ether and thiourea in another ethylene glycol methyl ether solvent, and then a two-step heat treatment process of sulfidation followed by selenization resulted in large grain size CZTSSe absorbers. Fortunately, a record efficiency of 10.1% CZTS solar cells was fabricated by the EGME solution process at that time.[130] Additionally, Hadke *et al.* showed that Cd could change the properties of acceptor defects near the valence band, while Ag improved photovoltaic performance by reducing bulk non-radiative recombination; successfully, a full area PCE of 10.1% (effective area efficiency of 10.8%) was achieved under the double cation substitution of 5% Ag + 25% Cd. The device structure is shown in Fig. 8a.[18] In 2018, Shih-Hsiung Wu *et al.* developed a post-vulcanization process to adjust the composition ratio of sulfur and selenium in CZTSSe solar cells (Fig. 8b gives a three-stage process), and when the sulfur content was 40%, the efficiency of CZTSSe solar cells was 11.1%.[131] In 2020, Su *et al.* proposed an ITO/CdS/CZCTS/Mo/glass post-annealing process to promote the interdiffusion of interlayer elements (Cu, Zn, In, and Sn) in the device, resulting in increased electron and hole densities at the interface, reducing traps, deep-level defects and non-radiative recombination; the efficiency was up to 12.6%. Fig. 8c shows the time-resolved photoluminescence decay for CZCTS thin films at a 532 nm excitation wavelength.[132] In addition, Zhao *et al.* obtained a CZTSSe solar cell with a certified efficiency of 12.18% (at a bake temperature of 280 °C) by optimizing the baking temperature during spin coating in 2020, and the efficiency of this certification is the highest recorded efficiency so far in ethylene glycol methyl ether-based solvent. Fig. 8d demonstrates the CZTS precursor solution for the CZTSSe device.[120]

5.3. Extrinsic doping of EGME-based routes

In 2014, Su *et al.* obtained a device with an efficiency of 5.10% using a 1% Na-doped CZTS solar cell.[126] In 2015, Tai *et al.* achieved a PCE of 8.2% by doping Sb in the absorbers.[134] In 2015, Su *et al.* introduced Cd into CZTS films to partially replace Zn to form $Cu_2Zn_{1-x}Cd_xSnS_4$ (CZCTS) films, which could reduce the second phase of ZnS and improve the grain size, significantly improving the PCE of CZTS solar cell devices from 5.30% to 9.24% (an active area efficiency of 9.82%).[129] In 2016, Hsieh *et al.* doped alkali metal in molecular precursor solutions, founding smaller alkali metal atoms that could increase the carrier concentration with the characterization by drive-level capacitance profiling (DLCP), while larger alkali atoms were beneficial to form large grain, obtaining a CZTSSe solar cell with an efficiency of 8.04% by K doping.[135] In 2018, Hadke *et al.* achieved a PCE of 10.8% with a double cation substitution strategy by partially replacing Cu with Ag and partially replacing Zn with Cd.[18] In 2018, Xiao *et al.* proved that the effect of In alloying on the performance of CZTSSe(In) solar cells mainly comes from its effect on the hole concentration of CZSSe(In), and the formation energy of In_{Cu} + In_{Sn} defects is lower than that of In_{Sn}, and In could replace Cu and Sn to

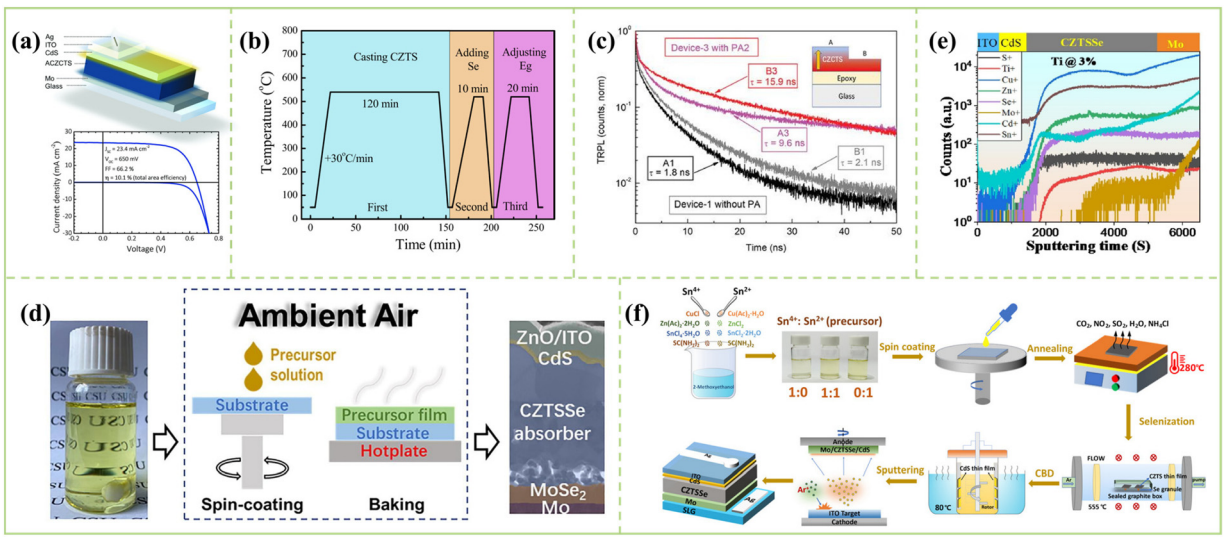

Fig. 8 (a) Light and dark IV characteristics of the champion ACZCTS device.[18] Copyright © 2018, WILEY-VCH Verlag GmbH & Co. KGaA. (b) Temperature profile of the three-stage process. First stage: Casting CZTS films; Second stage: selenization; and Third stage: post-sulfurization.[131] Copyright © 2018, Elsevier. (c) Time-resolved photoluminescence decay at 532 nm excitation wavelength for CZCTS thin films exfoliated from device-1 and device-3; the inset illustrates two depths of A (near Mo) and B (near CdS) in CZCTS thin film.[132] Copyright © 2020, WILEY-VCH Verlag GmbH & Co. KGaA. (d) Flow chart from the CZTS precursor solution to the CZTSSe device. Inside the dashed frame is the fabrication of CZTS precursor film through spin-coating and baking in the ambient air.[120] Copyright © 2020, Elsevier. (e) TOF-SIMS analysis of Ti-doped CZTSSe devices.[133] Copyright © 2022, Elsevier. (f) Schematic illustration of the fabrication process of CZTSSe thin film solar cells by optimizing the ratio of Sn^{4+} and Sn^{2+}.[34] Copyright © 2021, Wiley-VCH GmbH.

form In_{Cu} + In_{Sn} defects, resulting in lower PCE of In-doped CZTSSe solar cells.[136] In 2020, Ibrahim *et al.* fabricated CZTS (ACZTS-KCZTS) absorbers by silver alloy and potassium doping, achieving device efficiency of 8.24% by J_{SC} and V_{oc} improvement.[137] In addition to the above studies, Lie *et al.* found that for sulfides, CZTS + 4-layer $CM_{0.15}Z_{0.85}TS$ achieved the highest efficiency of 5.73% compared with the samples of CZTS by Mn substitution. However, in the sulfide selenide system, the highest cell performance of 8.74% was achieved using CZTSSe + 2-layer $CM_{0.15}Z_{0.85}TSSe$, showing that the Mn top substitution layer increased the depletion region width and short-wavelength collection.[138] In 2022, Liang *et al.* found that the introduction of Ti^{4+} into CZTSSe significantly improved the film morphology, increasing the grain size, and the PCE increased from 9.48% to 12.07%. The TOF-SIMS analysis of Ti-doped CZTSSe devices is given in Fig. 8e.[133] Subsequently, Chen *et al.* used the Ag, Ti dual-cation substitution to improve the device efficiency up to 12.73%.[139] In addition, Liang *et al.* also obtained high-quality CZTSSe films by optimizing the ratio of Sn^{4+}/Sn^{2+} in the CZTSSe precursor solution (the ratio of Sn^{4+}/Sn^{2+} = 1 : 1) (Fig. 8f), which reduces the concentration of deep defects, fortunately, achieving efficiency of over 11%.[34] In addition, Zhao *et al.* reported a simple and environmentally friendly additive strategy by adding water additives, which can improve the homogeneity and thermogravimetric characteristics of the precursor solution by adjusting the particle size and coordination behavior of the precursor solution, achieving a certified CZTSSe device with a PCE of 12.07%.[140] In 2022, an efficiency of 12.87% was achieved using a two-step cooling strategy, which can suppress the Cu_{Zn} and Sn_{Zn} defects and defect clusters synergistically.[141]

Unlike amine–thiol, DMSO and other solvents, the fabrication of CZTSSe solars by EGME solvent is not only insensitive to oxygen and water in the air but also does not show decomposition or uneven morphology. Moreover, the precursor solution configuration process, including the spin coating process and annealing process by this solvent system, can be operated in the air. In addition, the precursor solution is quite stable in the air. Because the preparation process of precursor thin film does not need vacuum equipment (such as a glove box), it can greatly reduce production costs and facilitate large-scale industrial production in the future.

6. Thioglycolic acid (TGA)-ammonia solution (NH_3H_2O)

6.1. Route origins and dissolution chemistry

Thioglycolic acid (TGA) is the most promising water-soluble ligand for CZTSSe precursors. Amazingly, this solvent not only has a lower GHS risk level, and lower cost but is also more active than other alkyl thiols with longer alkyl chains. Additionally, metal ions have a stronger coordination ability in this system, which is a key factor in the dissolution of metal oxides. In 2014, Tang's group reported a novel *in situ* self-stabilizing process using water to obtain CZTS nanoinks and finally achieved a very encouraging device efficiency of 5.14%.[142] In 2014, Tian *et al.* developed a multifunctional organic solvent composed of ethylene glycol methyl ether, thioglycolic acid and ethanolamine to dissolve metal oxides, metal hydroxides, metal chlorides, metal acetates, and metal acetylacetonates. Simultaneously, they used Cu, Zn, and Sn divalent oxides (*i.e.* CuO, ZnO and SnO) dissolved in a mixed solvent to prepare a CZTS precursor solution and achieved a PCE of 6.83%; the dissolution mechanism and the dissolved solution picture are depicted in Fig. 9a.[35] In 2015, a green, simple and stable precursor solution method based on water and ammonium thioglycolate aqueous solution was creatively proposed using ammonium thioglycolate aqueous solution and deionized water to dissolve Cu, Zn and Sn oxides; a pale yellow clear solution of CZTS was obtained (Fig. 9b). However, this mixed solvent system also can dissolve other metal oxides and metal hydroxides (CuO, ZnO, SnO, GeO_2, In_2O_3, Sb_2O_3, MgO, CdO, MnO, Bi_2O_3, Fe_2O_3, NiO, LiOH, NaOH, and KOH) in air at room temperature (Fig. 9b).[143] In 2015, Yang *et al.* proposed a mixed solution of thioglycolic acid and ethanolamine to dissolve Cu, Zn, Sn and Se metal powders, while ethylene glycol methyl ether was used to adjust the concentration and viscosity of the CZTSe precursor solution. Consequently, a clear and uniform CZTSe precursor solution was obtained, and the final pure selenide CZTSe solar cell obtained an efficiency of 8.02% (without anti-reflection coating). This is the first report on the simultaneous dissolution of elemental Cu, Zn, Se, and Sn powders (Fig. 9c).[144] More interestingly, other metal powders, such as Ga, In, Mg, Fe, Co, Ni, and Mn, can also be dissolved using this method. In 2016, Yang *et al.* of Pan's group first introduced the thioglycolic acid-ammonia system into the study of CZTSSe solar cells and obtained 6.96% efficiency by introducing Na doping, demonstrating that Cu, Zn, Sn, and S powders can be easily dissolved in aqueous solutions of thioglycolic acid and methylamine. Interestingly, besides Cu, Zn, Sn, and S powders, other elemental powders, such as Mg, Fe, Co, Ni, Se, In, Sb, and Mn, can also be dissolved in this system, and the dissolution diagram is shown in Fig. 9d, which opens up new avenues for the deposition of various metal chalcogenide films.[145] Thus far, record PCE of 12.8% (certified cell efficiencies) have been reported from TGA molecular inks in 2021 (Table 5).[146]

6.2. PV applications for thioglycolic acid-ammonia solution routes

In 2018, Tian *et al.* proposed an environment friendly aqueous solution process based on ammonium thioglycolate (TGAm), achieving 7.38% efficiency CZTS solar cells in ambient air.[149] Subsequently, Meng's group studied solvent coordination engineering, precursor component engineering and selenization crystallization kinetics to improve the performance of CZTSSe solar cells by employing a TGA solvent system and made very gratifying progress. In 2020, the coordination structure of metal-TGA in Cu–Zn–Sn–S aqueous precursor solution was systematically designed (Fig. 9e), achieving 12.3% efficiency and 12.0% certified efficiency owing to the better

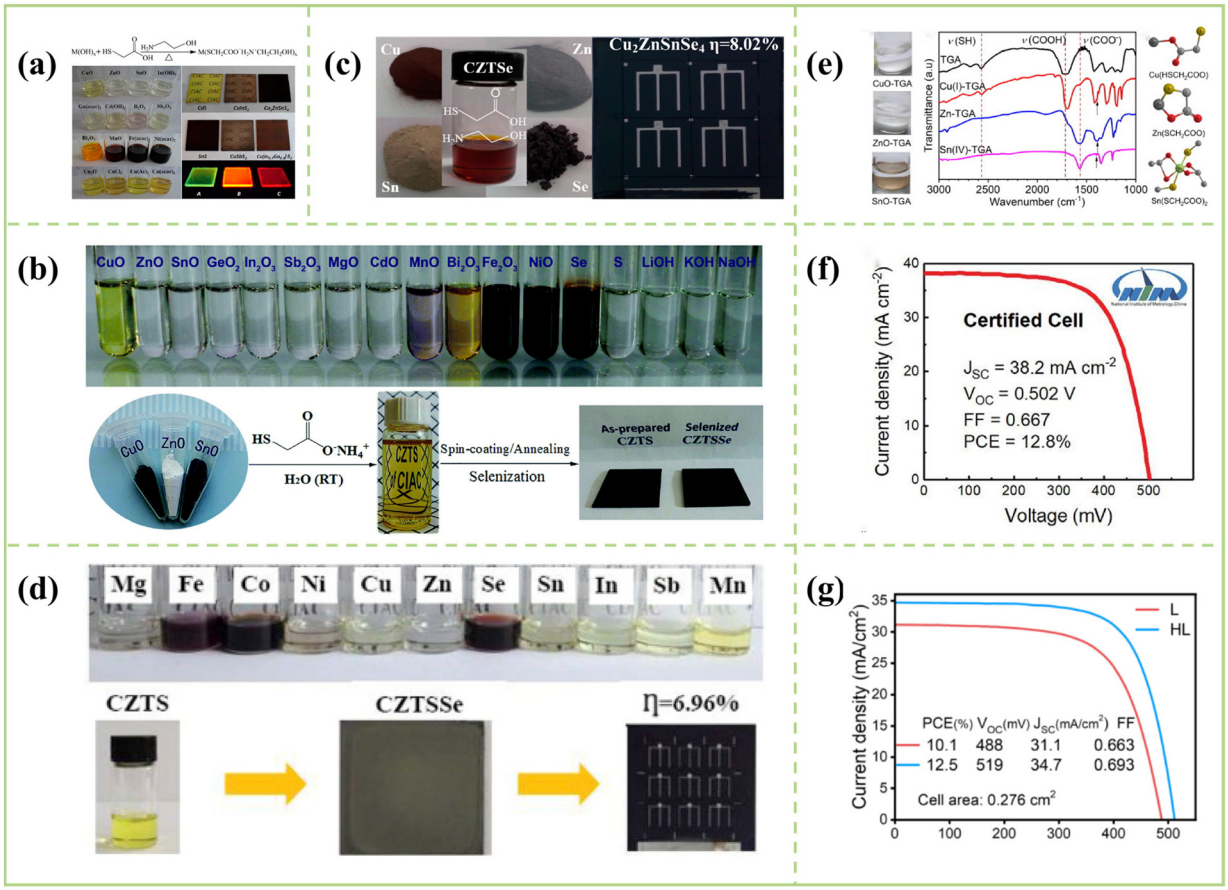

Fig. 9 (a) (Top) Dissolution mechanism of metal hydroxides in thioglycolic acid and ethanolamine; (bottom) digital pictures of various metal–organic precursor solutions as well as as-prepared CdS, $CuInS_2$, Cu_2ZnSnS_4, SnS, $CuSbS_2$, and $Cu(In_{0.7}Ga_{0.3})S_2$ nanocrystal thin films on glass substrates; samples A, B, and C are directly fabricated by Ag-doped $Zn_xCd_{1-x}S$ luminescent quantum dot thin films with a Zn/Cd ratio of 5 : 1, 3 : 1, and 1 : 1, respectively.[35] Copyright © 2014 American Chemical Society. (b) (Top) Digital photograph of a series of precursor solutions by dissolving metal oxides, metal hydroxides, selenium or sulfur in the aqueous solution of ammonium thioglycolate. (Bottom) A schematic illustration of the formation of the CZTS precursor solution, CZTS, and CZTSSe thin films.[143] Copyright © 2015, Royal Society of Chemistry. (c) Precursor solutions and devices by the dissolution of elemental Cu, Zn, Sn, and Se powders.[144] Copyright © 2014, American Chemical Society. (d) Photograph of Mg, Fe, Co, Ni, Cu, Zn, Se, In, Sb, and Mn precursor aqueous solutions (~0.2 M) by dissolving the corresponding elemental powders in the aqueous solution of thioglycolic acid and methylamine.[145] Copyright © 2016, Elsevier. (e) Chemical reactions between metal oxides and TGA.[147] Copyright © 2020, Elsevier. (f) Current–voltage of the champion cell measured in a photovoltaic certified organization (National Institute of Metrology, China).[146] Copyright © 2021 Wiley-VCH GmbH. (g) *J*–*V* characteristics of the champion cells.[148] Copyright © 2022, Royal Society of Chemistry.

conditions for nucleation and crystallization.[147] In 2021, Meng's group also found that the high composition tolerance is mainly due to the existence of the conductive carbon framework layer with high element accommodation capacity. The phase-separated growth behavior of CZTSSe grains is driven by the thermodynamic properties of the multiphase thin film system and the coordination structure-induced formation of large metal–organic clusters, but Sn has a six-coordination structure and deprotonated TGA with two-coordinate end groups; finally, certified efficiency of 12.8% was achieved (effective area of 13.5%) (Fig. 9f).[146] In 2022, a two-step selenization strategy was developed to control the growth kinetics of aqueous solution-derived CZTSSe films and achieved 12.5% high-efficiency kesterite solar cell (Fig. 9g).[148]

The advantages of the CZTSSe precursors by aqueous solution (Thioglycolic acid/ammonia) are safe, low-cost and environment-friendly. In addition, the aqueous solution system is constructed using ammonia instead of amine, and the precursor solution is obtained by dissolving metal oxides, which reduces the carbon content and is conducive to high-quality CZTSSe thin films. Compared with DMSO/DMF, TGA not only has a stronger coordination ability with metal ions but also the precursor solution is more stable. This ultra-stable precursor solution provides a more favorable time window for the fabrication of CZTSSe solar cells.

7. Discussion—performance comparison of high-efficiency devices

In this section, the device performance of the highest PCE obtained from seven processes for CZTSSe absorbers, namely

Table 5 A selected summary of precursor ink formulations, heat treatments, and device performances for $Cu_2ZnSn(S,Se)_4$ solar cells using thioglycolic acid–ammonia-based precursor solution method (TGA)-deposited absorbers. PCE is the total area unless otherwise stated

Year	Solar cell	Molecular ink	Dissolution condition	Heat treatments	Area [cm^2]	V_{OC} [mV]	J_{SC} [mA cm^{-2}]	FF [%]	PCE [%]	Institute	Ref.
2016	CZTSSe	Cu Zn, Sn and S, dissolved in the mixed solution of thioglycolic acid and methylamine	Stirred (45 °C)	Annealed (510 °C)	0.19	378	28.17	65.4	6.96[a]	CIAC	145
2018	CZTSSe	SnO of $TGAm_{aq}$ + CuO, ZnO of deionized water was dripped into the above solution and homogenous CZTS precursor solution was obtained	Stirred (50 °C)	Annealed (540 °C)	0.21	420	30.54	57.01	7.38[a]	SXNU	149
2020	CZTSSe	CuO, ZnO and SnO in a mixture of aqueous solutions of TGA and NH_3 H_2O	Stirred (60 °C)	Selenized (520 °C)	0.18	487	36.5	69.3	12.3[a,b]	IOP, CAS	147
2021	CZTSSe	CuO, ZnO and SnO in a mixture of 1.2 ml TGA and 2.6 ml $NH_3{\cdot}H_2O$	Stirred (60 °C)	Annealed (520 °C)	0.18	502	38.2	66.7	12.8[b,c]	IOP, CAS	146
2022	CZTSSe	CuO, ZnO and SnO in a mixture of 1.2 ml TGA and 2.6 ml $NH_3{\cdot}H_2O$	Stirred (60 °C)	Annealed (570 °C + 510 °C)	0.276	519	34.7	69.3	12.5[b]	IOP, CAS	148

[a] Active area. [b] Cells with ARC. [c] Certified cell efficiencies.

vacuum-deposited absorbers (CZTSSe (V), η = 12.62%),[25] absorbers from hydrazine-based (CZTSSe (H), η = 12.6%),[30] absorbers from amine–thiol-based (CZTSSe (A), η = 12.54%),[65] DMSO-based processes (CZTSSe (D), η = 13.0%),[24] DMF-based processes (CZTSSe (M), η = 12.25%),[117] EGME-based processes (CZTSSe (E), η = 12.18%)[120] and TGA-based processes (CZTSSe (T), η = 12.8%),[146] are discussed. Kim's vacuum-processed CZTSSe solar cells achieved world record efficiency using (i) an optimized SLG-Mo/Zn/Cu/Sn (MZCT) as the stacking structure to clarify the elemental volatilization of Zn using the MZCT stacking structure, (ii) using hydrogen sulfide gas (H_2S) to effectively control the S/(S + Se) ratio of the films in the sulfoselenization process and suppress the volatilization of Zn, and (iii) an optimized annealing process.[25] The optimization of the heat treatment process is not only the key aspect of band gap engineering but also is particularly valuable at the device interfaces for achieving an optimum band alignment, controlling interface defects and recombination, and optimizing the formation of carrier-selective contacts.[117,150]

The properties of the CZTS precursor solution are crucial for high-quality absorbers.[151] Compared with the slurry process, the rheological properties of the particle-free solution using the hydrazine pure solution method significantly improved the uniformity and structure by Mitzi. Furthermore, the thicknesses of the TCO and cadmium sulfide are optimized at the same time to maximize the transmission of photons to the absorbers, thus improving the performance of solar cells. In particular, the J_{SC} and V_{OC} have been improved to 12.6% of the champion devices.[30] Similarly, cation doping/substitution strategies have been also used to improve the performance of CZTSSe devices.[18,152–156] The Ag^+ substitution for Cu^+ has been shown to significantly improve device performance by not only suppressing or eliminating the Cu/Zn disorder in CZTSSe materials, which reduces the density of harmful defects, but also modulating the energy band structure of CZTSSe, changing the optical band gap of CZTSSe films, improving the energy band deviation value of the PN heterojunction, increasing the ability of electron transition, optimizing the open-circuit voltage of the devices, effectively increasing the photoluminescence quantum yield (PLQY), and prolonging the carrier lifetime of the devices.[99,157–159] In 2021, the efficiency of devices made with 10% silver alloying is as high as 13.0% (NREL certification).[24] Amazingly, the efficiency of several other solvent systems has also been greatly improved. The following sections carefully explain the differences in device PCEs by examining the individual performance parameters of the seven cells, including V_{OC}, short-circuit current density (J_{SC}), and FF in more detail.

7.1. Open-circuit voltage analysis

CZTSSe (V) prepared by vacuum-deposited absorbers has the highest open-circuit voltage (541.1 mV) with an efficiency of 12.62% (ARC, effective area) (Fig. 10b).[25] In contrast, devices with solution-based absorbers are limited by open-circuit voltage, meaning that CZTSSe (E) prepared by EGME-based absorbers has the lowest open-circuit voltage (465.1 mV). The V_{OC} of hydrazine, DMSO, DMF, amine–thiol and TGA ink-based devices is 5%, 2%, 10%, 11% and 7% lower than vacuum deposition devices, respectively.[24,30] For CZTSSe (V) devices, the authors attributed the high V_{OC} to the hydrogen sulfide gas used in sulfur selenization, leading to the gradient band gap of the CZTSSe absorbers, reducing the non-radiative recombination.[25] For CZTSSe (H) devices, more significant improvements in device performance remain the further reduction of the V_{oc} deficit.[30] For CZTSSe (A) devices, the lower V_{oc} may be due to the serious non-radiative recombination caused by the fine grain layer in the middle of the absorber. If the crystallinity of the absorber structure can be further

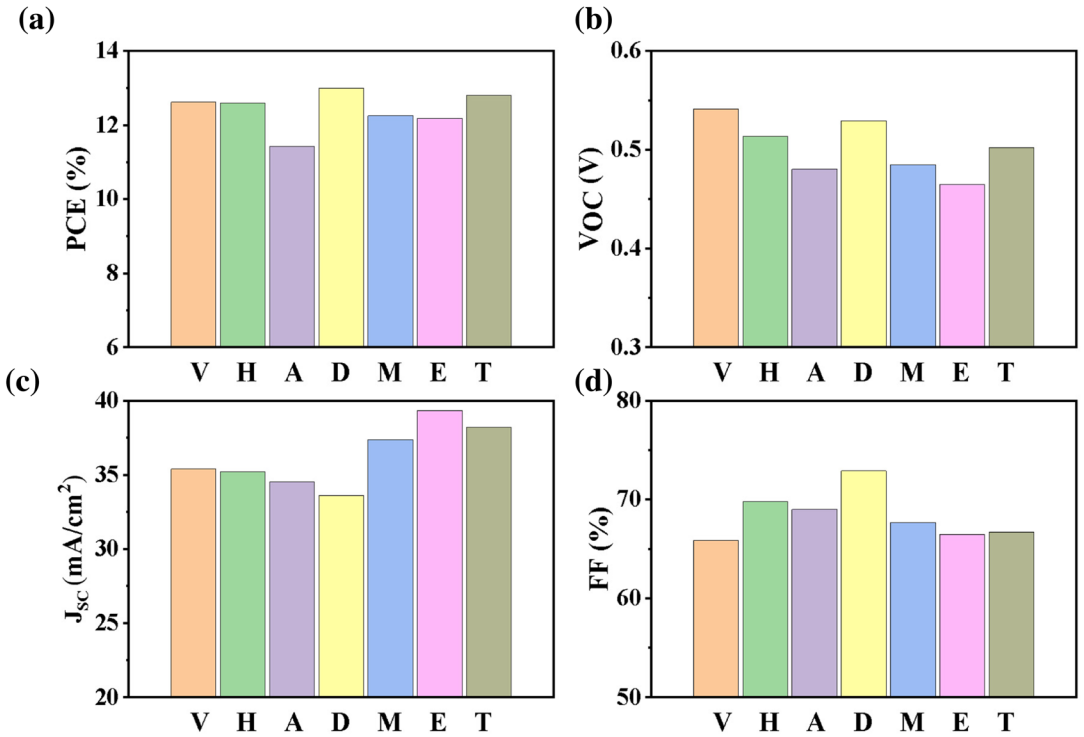

Fig. 10 (a–d) Experimental device performance values for efficiency, V_{OC}, J_{SC}, and FF for champion vacuum[25] and solution-processed CZTSSe (H,[30] A,[65] D[24], M,[117] E,[120] and T[146]) solar cells, respectively.

improved, the efficiency of this solvent system will be significantly improved. The V_{OC} value of 529.4 mV is obtained using DMSO. However, the V_{oc} and filling factor (FF) of the devices can be significantly improved only by low-temperature heat treatment of the ACZTSSe/CdS heterojunction.[24] Moreover, devices with DMF-based absorbers have lower V_{OC} compared with DMSO. Although the DMF and DMSO coordination structures are similar, the main reason for this difference may be the raw material valence state of the precursor solution or the phase transition caused by the chemical reaction pathway. For CZTSSe (E) devices, its lowest V_{oc} may be similar to amine–thiol-based absorbers. Even though the certified efficiency of the TGA system is almost equivalent to that of DMSO, the V_{OC} of the TGA system is 27.4 mV lower than that of DMSO. The main reason for this difference may be that DMSO is a double layer of large grains, while there is a graphitized layer of fine grains at the bottom of the TGA absorbers.

7.2. Current density analysis

Unlike V_{OC}, the short-circuit current density (J_{SC}) of EGME-based CZTSSe (E) is the highest among solution-processed devices and exceeds that of vacuum-processed devices. In contrast, the J_{SC} of DMSO-based devices is the lowest among solution-processed devices; its J_{SC} is only 33.58 mA cm^{-2}. Furthermore, hydrazine-based devices are almost the same as those of vacuum-based devices, only 0.5% lower than vacuum, while the J_{SC} of amine–thiol-based devices and TGA-based devices are 12% and 3% lower than EGME-deposited devices, respectively, suggesting that CZTSSe (EGME) has better light absorption and carrier collection under the condition of short circuit. Currently, DMSO devices have the highest certified efficiency, but their J_{sc} of performance parameters is the lowest of all manufacturing methods, which may significantly limit the efficiency improvement of the device. Compared with the loss of V_{OC}, the loss of J_{SC} is lower; however, it undoubtedly provides room for device performance improvement.[160]

7.3. Fill factor analysis

In addition to the difference between V_{OC} and J_{SC}, the fill factor of the device fabricated by hydrazine and DMSO is 6% and 11%, respectively, higher than that of CZTSSe (V), especially the device fabricated by DMSO has a fill factor as high as 72.9%.[24,25,30] Currently, the highest certified efficiency by DMSO is 13.0% from NREL, which may be related to the increase in FF value, meaning that the grain boundary in CZTSSe (D) is relatively mild or good passivation but has only little contribution to the recombination in the device.[24] However, vacuum processes, such as sputtering, are based on the mutual diffusion of high-purity elements, Cu, Zn, Sn and Se/S. For example, the magnetron sputtering method is sputtered on the Mo-SLG substrate by DC sputtering at room temperature to form a metal precursor with Zn/Cu/Sn sequence and then converted to CZTSSe by sulfuration/selenization.[161–163] In contrast, the solution-processed method usually requires a direct coating of a single precursor ink containing almost all the elements (Cu, Zn, Sn and S/Se) in the mixed atomic com-

position, which is deposited, annealed and then converted into CZTSSe thin films in S/Se atmosphere.[164,165] Notably, CZTSSe phases in solvent systems may introduce additional elemental impurities (*e.g.*, C, O, N, and Cl) that remain in the final deposited films and may be harmful to the bulk materials (*e.g.* double layers and/or fine grains) and electrical qualities (low shunt and high series resistance).[96,120] Furthermore, it may be challenging to achieve an ideal and controllable bandgap gradient through the selenization of elemental metal (Cu, Zn, and Sn) precursors. Therefore, the inherent differences in growth and phase transition mechanisms between vacuum and solution-processed methods may contribute to the existence of more electroactive defects in kesterite solar cells using the solution method, affecting the V_{OC} and J_{SC} of the device through residual solvent impurities (*e.g.* carbon), impurity deposition introduced during the film process (*e.g.* oxygen) and uneven film composition.

8. Outlook

In summary, CZTSSe solar cells have exhibited great potential and great progress using the solution method in the past few decades. Solution processing techniques offer simple operation processing, low-cost processing, high throughput and excellent material utilization.[44,94,96] However, to achieve a wider range of applications, they must compete with existing technologies in terms of efficiency and solving possible toxicity problems. This paper mainly reviews the molecular ink deposition technology of CZTSSe.

The efficiency of two molecular ink technologies based on hydrazine and DMSO solvents has been proven to be more than 12% following several years of development. Hydrazine solution does not need selenization and is in a leading position in terms of performance and device quality.[30] In contrast, DMSO-based processes require selenization, achieving a record efficiency of 13.0% (certified by NREL).[24] In addition, the other four solvent systems achieve the device efficiency of CZTSSe in the range of 11–13%, namely amine–thiol-based devices: 12.54% (Wu's group),[65] TU/DMF-based devices: 12.25% (Zhang's group),[117] EGME-based devices: 12.73% (Su's group),[139] and TGA-based devices: 12.8% (Meng's group, certified efficiency).[146] Solution deposition techniques demonstrate their ability to create controllable, dense and high-quality kesterite absorbers for photovoltaic applications, especially DMSO and TGA solvents. However, further improvements in device performance are essential for upgrading to large-scale commercial production.

(i) Advanced processes, such as postdeposition alkali treatment (alkali metals, including Li, Na, and K), have been shown to improve device efficiency, and the adoption of the solution processing route needs to be combined with the base process to better improve device performance. In addition, there is an opportunity for solution-processed devices to play a leading role, as dopants can be added directly to the precursor ink, thereby avoiding the contamination of expensive deposition equipment.[79,166]

(ii) Carbon is a well-known impurity that usually increases the series resistance of devices by forming a charge barrier to the back contact. On the contrary, some researchers have reported that carbonaceous impurities are benign and contribute to the high component tolerance of thin films. Therefore, to further develop the potential of these processes, it is necessary to understand the harmful impurities in CZTSSe absorbers and the level of their tolerable concentrations.[146,167]

(iii) Currently, developed optimization techniques, such as buffer layer replacement, alkali metal doping, cation substitution, gradient band gap, selenization process improvement and other optimization methods, have achieved satisfactory results; however, the efficiency still does not reach the commercial level.[79,168–171] The performance of the absorbers and the photovoltaic performance of the solar cells mainly depends on the composition of the precursor film and the reaction pathway of the transition from the precursor to the absorbers. Therefore, future research will focus on the solution chemical reaction pathway, finding the optimal direction to effectively reduce the intrinsic defects of CZTSSe absorbers.[151,172,173]

(iv) Theoretically and experimentally confirming that Sn-related deep defects are the main reasons for limiting CZTSSe devices. To further promote the development of CZTSSe solar cells, it is urgent to study deeply the formation mechanism and passivation strategy of Sn-related deep-level defects. It is very important to fully understand the CZTSSe bulk phase of Sn-related deep-level defects and its effects on photovoltaic performance.[9,174–178]

This review systematically summarizes the advanced development of solution-processed kesterite solar cells. Solvent plays an important role in solution-processed kesterite solar cells because it not only acts as a precursor dissolution medium but also governs the crystallization process. Simultaneously, solution processing routes have demonstrated the most promising results for kesterite absorbers, and exciting efficiencies can certainly be achieved in future developments.

Conflicts of interest

The authors declare no conflict of interest.

Acknowledgements

This work was financially supported by the National Natural Science Foundation of China (Grant No. 62074052, U1904192, 62104061, 61974173 and 61874159) and the Science and Technology Innovation Talents in Universities of Henan Province (21HASTIT023).

References

1 Y.-M. Wei, K. Chen, J.-N. Kang, W. Chen, X.-Y. Wang and X. Zhang, *Engineering*, 2022, **14**, 52–63.

2 U. K. Das, K. S. Tey, M. Seyedmahmoudian, S. Mekhilef, M. Y. I. Idris, W. Van Deventer, B. Horan and A. Stojcevski, *Renewable Sustainable Energy Rev.*, 2018, **81**, 912–928.
3 G. Liu, J. Xu, T. Chen and K. Wang, *Phys. Rep.*, 2022, **981**, 1–50.
4 M. A. Green, E. D. Dunlop, J. Hohl-Ebinger, M. Yoshita, N. Kopidakis, K. Bothe, D. Hinken, M. Rauer and X. Hao, *Prog. Photovolt.: Res. Appl.*, 2022, **30**, 687–701.
5 A. Polizzotti, I. L. Repins, R. Noufi, S. H. Wei and D. B. Mitzi, *Energy Environ. Sci.*, 2013, **6**, 3171.
6 H. Zhou, W. C. Hsu, H. S. Duan, B. Bob, W. Yang, T. B. Song, C. J. Hsu and Y. Yang, *Energy Environ. Sci.*, 2013, **6**, 2822.
7 D. Shin, B. Saparov and D. B. Mitzi, *Adv. Energy Mater.*, 2017, **7**, 1602366.
8 Y. Ren, M. Richter, J. Keller, A. Redinger, T. Unold, O. Donzel-Gargand, J. J. S. Scragg and C. P. Björkman, *ACS Energy Lett.*, 2017, **2**, 976–981.
9 S. K. Wallace, D. B. Mitzi and A. Walsh, *ACS Energy Lett.*, 2017, **2**, 776–779.
10 R. Fonoll-Rubio, J. Andrade-Arvizu, J. Blanco-Portals, I. Becerril-Romero, M. Guc, E. Saucedo, F. Peiró, L. Calvo-Barrio, M. Ritzer, C. S. Schnohr, M. Placidi, S. Estradé, V. Izquierdo-Roca and A. Pérez-Rodríguez, *Energy Environ. Sci.*, 2021, **14**, 507–523.
11 X. Zhang, D. Han, S. Chen, C. Duan and J. Chu, *J. Energy Chem.*, 2018, **27**, 1140–1150.
12 C. Wang, S. Chen, J.-H. Yang, L. Lang, H.-J. Xiang, X.-G. Gong, A. Walsh and S.-H. Wei, *Chem. Mater.*, 2014, **26**, 3411–3417.
13 M. Nakamura, K. Yamaguchi, Y. Kimoto, Y. Yasaki, T. Kato and H. Sugimoto, *IEEE J. Photovolt.*, 2019, **9**, 1863–1867.
14 Z. Xu, Q. Gao, C. Cui, S. Yuan, D. Kou, Z. Zhou, W. Zhou, Y. Meng, Y. Qi, M. Ishaq, U. A. Shah and S. Wu, *Adv. Funct. Mater.*, 2022, 2209187.
15 K. Woo, Y. Kim and J. Moon, *Energy Environ. Sci.*, 2012, **5**, 5340–5345.
16 Y. Cao, M. S. Denny, J. V. Caspar, W. E. Farneth, Q. Guo, A. S. Ionkin, L. K. Johnson, M. Lu, I. Malajovich, D. Radu, H. D. Rosenfeld, K. R. Choudhury and W. Wu, *J. Am. Chem. Soc.*, 2012, **134**, 15644–15647.
17 P. Martínez-Ortiz, J. F. Trigo, N. Pineda-Aguilar and C. Guillén, *Mater. Res. Bull.*, 2022, **152**, 111844.
18 S. H. Hadke, S. Levcenko, S. Lie, C. J. Hages, J. A. Márquez, T. Unold and L. H. Wong, *Adv. Energy Mater.*, 2018, **8**, 1802540.
19 K. Sun, J. Huang, C. Yan, A. Pu, F. Liu, H. Sun, X. Liu, Z. Fang, J. A. Stride, M. Green and X. Hao, *Chem. Mater.*, 2018, **30**, 4008–4016.
20 M. Ravindiran and C. Praveenkumar, *Renewable Sustainable Energy Rev.*, 2018, **94**, 317–329.
21 S. Suresh and A. R. Uhl, *Adv. Energy Mater.*, 2021, **11**, 2003743.
22 Y. Liu, B. Xu, X. Lu, X. Qin, P. Yang, J. Chu, Y. Chen and L. Sun, *Sol. Energy*, 2021, **215**, 451–458.
23 B. I. Park, Y. Hwang, S. Y. Lee, J. S. Lee, J. K. Park, J. Jeong, J. Y. Kim, B. Kim, S. H. Cho and D. K. Lee, *Nanoscale*, 2014, **6**, 11703–11711.
24 Y. Gong, Q. Zhu, B. Li, S. Wang, B. Duan, L. Lou, C. Xiang, E. Jedlicka, R. Giridharagopal, Y. Zhou, Q. Dai, W. Yan, S. Chen, Q. Meng and H. Xin, *Nat. Energy*, 2022, **7**, 966–977.
25 D.-H. Son, S.-H. Kim, S.-Y. Kim, Y.-I. Kim, J.-H. Sim, S.-N. Park, D.-H. Jeon, D.-K. Hwang, S.-J. Sung, J.-K. Kang, K.-J. Yang and D.-H. Kim, *J. Mater. Chem. A*, 2019, **7**, 25279–25289.
26 M. A. Green, E. D. Dunlop, G. Siefer, M. Yoshita, N. Kopidakis, K. Bothe and X. Hao, *Prog. Photovolt.: Res. Appl.*, 2022, **31**, 3–16.
27 S. Ge, H. Xu, Y. Huang, S. K. Karunakaran, R. Hong, J. Li, Y. Mai, E. Gu, X. Lin and G. Yang, *Sol. RRL*, 2020, **4**, 2000325.
28 P. Punathil, S. Zanetti, E. Artegiani, V. Kumar and A. Romeo, *Sol. Energy*, 2021, **224**, 992–999.
29 T. K. Todorov, K. B. Reuter and D. B. Mitzi, *Adv. Mater.*, 2010, **22**, 156–159.
30 W. Wang, M. T. Winkler, O. Gunawan, T. Gokmen, T. K. Todorov, Y. Zhu and D. B. Mitzi, *Adv. Energy Mater.*, 2014, **4**, 1301465.
31 L. Lou, Y. Gong, J. Zhou, J. Wang, X. Xu, K. Yin, B. Duan, H. Wu, J. Shi, Y. Luo, D. Li, H. Xin and Q. Meng, *J. Energy Chem.*, 2022, **70**, 154–161.
32 J. Zhao, Y. Zhao, X. Tan, W. Liu, W. Zhao, Y. Fang and X. Han, *Sol. Energy Mater. Sol. Cells*, 2021, **226**, 111092.
33 Y. Guo, J. Zhu, D. Kou, W. Zhou, Z. Zhou, S. Yuan, Y. Qi, Y. Meng, L. Han, Z. Zheng and S. Wu, *ACS Appl. Mater. Interfaces*, 2022, **14**, 26690–26698.
34 G.-X. Liang, Z.-X. Yu, Z.-G. Xie, Y. He, J.-H. Lin, S. Chen, Z.-H. Zheng, J.-T. Luo, P. Fan, Z.-H. Su, H.-L. Ma and X.-H. Zhang, *Sol. RRL*, 2021, **5**, 2100574.
35 Q. Tian, G. Wang, W. Zhao, Y. Chen, Y. Yang, L. Huang and D. Pan, *Chem. Mater.*, 2014, **26**, 3098–3103.
36 J. Li, Y. Huang, J. Huang, G. Liang, Y. Zhang, G. Rey, F. Guo, Z. Su, H. Zhu, L. Cai, K. Sun, Y. Sun, F. Liu, S. Chen, X. Hao, Y. Mai and M. A. Green, *Adv. Mater.*, 2020, **32**, 2005268.
37 J. Li, J. Huang, J. Cong, Y. Mai, Z. Su, G. Liang, A. Wang, M. He, X. Yuan, H. Sun, C. Yan, K. Sun, N. J. Ekins-Daukes, M. A. Green and X. Hao, *Small*, 2022, **18**, 2105044.
38 S.-Y. Kim, D.-H. Son, S.-H. Kim, Y.-I. Kim, S. Kim, K. Ahn, K.-J. Yang, J.-K. Kang and D.-H. Kim, *Adv. Energy Mater.*, 2020, **10**, 1903173.
39 D. Wang, W. Zhao, Y. Zhang and S. Liu, *J. Energy Chem.*, 2018, **27**, 1040–1053.
40 D. B. Mitzi, *Adv. Mater.*, 2009, **21**, 3141–3158.
41 D. B. Mitzi, M. Yuan, W. Liu, A. J. Kellock, S. J. Chey, L. Gignac and A. G. Schrott, *Thin Solid Films*, 2009, **517**, 2158–2162.
42 D. B. Mitzi, M. Yuan, W. Liu, A. J. Kellock, S. J. Chey, V. Deline and A. G. Schrott, *Adv. Mater.*, 2008, **20**, 3657–3662.

43 M. Yuan and D. B. Mitzi, *Dalton Trans.*, 2009, 6078–6088.
44 J. Guo, Y. Pei, Z. Zhou, W. Zhou, D. Kou and S. Wu, *Nanoscale Res. Lett.*, 2015, **10**, 1045.
45 R. Zhang, S. M. Szczepaniak, N. J. Carter, C. A. Handwerker and R. Agrawal, *Chem. Mater.*, 2015, **27**, 2114–2120.
46 G. Wang, W. Zhao, Y. Cui, Q. Tian, S. Gao, L. Huang and D. Pan, *ACS Appl. Mater. Interfaces*, 2013, **5**, 10042–10047.
47 N. S. Arul, D. Y. Yun, D. U. Lee and T. W. Kim, *Nanoscale*, 2013, **5**, 11940–11943.
48 W. Li, Z. Su, J. M. R. Tan, S. Y. Chiam, H. L. Seng, S. Magdassi and L. H. Wong, *Chem. Mater.*, 2017, **29**, 4273–4281.
49 G. Altamura and J. Vidal, *Chem. Mater.*, 2016, **28**, 3540–3563.
50 Z. Zhang, L. Yao, Y. Zhang, J. Ao, J. Bi, S. Gao, Q. Gao, M.-J. Jeng, G. Sun, Z. Zhou, Q. He and Y. Sun, *Adv. Sci.*, 2018, **5**, 1700645.
51 J. Liu, Q. Shen, Z. Liu, X. Gao, Z. Zhang, X. Liu, K. Cheng and Z. Du, *ACS Appl. Mater. Interfaces*, 2021, **13**, 31852–31860.
52 F.-I. Lai, J.-F. Yang, Y.-L. Wei and S.-Y. Kuo, *Green Chem.*, 2017, **19**, 795–802.
53 J. Park, H. Yoo, V. Karade, K. S. Gour, E. Choi, M. Kim, X. Hao, S. J. Shin, J. Kim, H. Shim, D. Kim, J. H. Kim, J. Yun and J. H. Kim, *J. Mater. Chem. A*, 2020, **8**, 14538–14544.
54 M. S. Kumar, S. P. Madhusudanan and S. K. Batabyal, *Sol. Energy Mater. Sol. Cells*, 2018, **185**, 287–299.
55 D. A. R. Barkhouse, O. Gunawan, T. Gokmen, T. K. Todorov and D. B. Mitzi, *Prog. Photovolt.: Res. Appl.*, 2012, **20**, 6–11.
56 S. Bag, O. Gunawan, T. Gokmen, Y. Zhu and D. B. Mitzi, *Chem. Mater.*, 2012, **24**, 4588–4593.
57 T. K. Todorov, J. Tang, S. Bag, O. Gunawan, T. Gokmen, Y. Zhu and D. B. Mitzi, *Adv. Energy Mater.*, 2013, **3**, 34–38.
58 W.-C. Hsu, B. Bob, W. Yang, C.-H. Chung and Y. Yang, *Energy Environ. Sci.*, 2012, **5**, 8564.
59 H.-S. Duan, W. Yang, B. Bob, C.-J. Hsu, B. Lei and Y. Yang, *Adv. Funct. Mater.*, 2013, **23**, 1466–1471.
60 M. T. Winkler, W. Wang, O. Gunawan, H. J. Hovel, T. K. Todorov and D. B. Mitzi, *Energy Environ. Sci.*, 2014, **7**, 1029–1036.
61 W. Yang, H. S. Duan, B. Bob, H. Zhou, B. Lei, C. H. Chung, S. H. Li, W. W. Hou and Y. Yang, *Adv. Mater.*, 2012, **24**, 6323–6329.
62 J. Zhong, Z. Xia, M. Luo, J. Zhao, J. Chen, L. Wang, X. Liu, D. J. Xue, Y. B. Cheng, H. Song and J. Tang, *Sci. Rep.*, 2014, **4**, 6288.
63 J. Kim, H. Hiroi, T. K. Todorov, O. Gunawan, M. Kuwahara, T. Gokmen, D. Nair, M. Hopstaken, B. Shin, Y. S. Lee, W. Wang, H. Sugimoto and D. B. Mitzi, *Adv. Mater.*, 2014, **26**, 7427–7431.
64 D. H. Webber and R. L. Brutchey, *J. Am. Chem. Soc.*, 2013, **135**, 15722–15725.
65 Y. Zhao, X. Zhao, D. Kou, W. Zhou, Z. Zhou, S. Yuan, Y. Qi, Z. Zheng and S. Wu, *ACS Appl. Mater. Interfaces*, 2021, **13**, 795–805.
66 X. P. Cui, Q. Ma, W. H. Zhou, D. X. Kou, Z. J. Zhou, Y. N. Meng, Y. F. Qi, S. J. Yuan, L. T. Han and S. X. Wu, *Nanoscale*, 2023, **15**, 185–194.
67 Y. Liu, D. Yao, L. Shen, H. Zhang, X. Zhang and B. Yang, *J. Am. Chem. Soc.*, 2012, **134**, 7207–7210.
68 D. H. Webber, J. J. Buckley, P. D. Antunez and R. L. Brutchey, *Chem. Sci.*, 2014, **5**, 2498–2502.
69 C. L. McCarthy, D. H. Webber, E. C. Schueller and R. L. Brutchey, *Angew. Chem., Int. Ed.*, 2015, **54**, 8378–8381.
70 Z. Lin, Q. He, A. Yin, Y. Xu, C. Wang, M. Ding, H.-C. Cheng, B. Papandrea, Y. Huang and X. Duan, *ACS Nano*, 2015, **9**, 4398–4405.
71 Y. Qi, Q. Tian, Y. Meng, D. Kou, Z. Zhou, W. Zhou and S. Wu, *ACS Appl. Mater. Interfaces*, 2017, **9**, 21243–21250.
72 J. C. Lowe, L. D. Wright, D. B. Eremin, J. V. Burykina, J. Martens, F. Plasser, V. P. Ananikov, J. W. Bowers and A. V. Malkov, *J. Mater. Chem. C*, 2020, **8**, 10309–10318.
73 J. Fu, D. Kou, W. Zhou, Z. Zhou, S. Yuan, Y. Qi and S. Wu, *J. Mater. Chem. A*, 2020, **8**, 22292–22301.
74 Q. Tian, Y. Cui, G. Wang and D. Pan, *RSC Adv.*, 2015, **5**, 4184–4190.
75 Q. Yan, S. Cheng, X. Yu, H. Jia, J. Fu, C. Zhang, Q. Zheng and S. Wu, *Sol. RRL*, 2019, **4**, 1900410.
76 Y. Deng, Z. Zhou, X. Zhang, L. Cao, W. Zhou, D. Kou, Y. Qi, S. Yuan, Z. Zheng and S. Wu, *J. Energy Chem.*, 2021, **61**, 1–7.
77 Q. Yan, Q. Sun, H. Deng, W. Xie, C. Zhang, J. Wu, Q. Zheng and S. Cheng, *J. Energy Chem.*, 2022, **75**, 8–15.
78 Y. Du, S. Wang, Q. Tian, Y. Zhao, X. Chang, H. Xiao, Y. Deng, S. Chen, S. Wu and S. Liu, *Adv. Funct. Mater.*, 2021, **31**, 2010325.
79 X. Chang, J. Fu, D. Kou, W. Zhou, Z. Zhou, S. Yuan, Y. Qi, Z. Zheng and S. Wu, *J. Mater. Chem. A*, 2021, **9**, 413–422.
80 H.-Q. Xiao, W.-H. Zhou, D.-X. Kou, Z.-J. Zhou, Y.-N. Meng, Y.-F. Qi, S.-J. Yuan, Q.-W. Tian and S.-X. Wu, *Green Chem.*, 2020, **22**, 3597–3607.
81 C. Cui, D. Kou, W. Zhou, Z. Zhou, S. Yuan, Y. Qi, Z. Zheng and S. Wu, *J. Energy Chem.*, 2022, **67**, 555–562.
82 W. Xie, Q. Sun, Q. Yan, J. Wu, C. Zhang, Q. Zheng, Y. Lai, H. Deng and S. Cheng, *Small*, 2022, **18**, 2201347.
83 S. Grini, K. V. Sopiha, N. Ross, X. Liu, T. S. Bjørheim, C. Platzer-Björkman, C. Persson and L. Vines, *Adv. Energy Mater.*, 2019, **9**, 1900740.
84 S. Zamulko, K. Berland and C. Persson, *Phys. Status Solidi A*, 2018, **215**, 1700945.
85 S. Zamulko, R. Chen and C. Persson, *Phys. Status Solidi B*, 2017, **254**, 1700084.
86 S. Berman, G. S. Gautam and E. A. Carter, *ACS Sustainable Chem. Eng.*, 2019, **7**, 5792–5800.
87 S. Hadke, S. Levcenko, G. S. Gautam, C. J. Hages, J. A. Márquez, V. Izquierdo-Roca, E. A. Carter, T. Unold and L. H. Wong, *Adv. Energy Mater.*, 2019, **9**, 1902509.

88 R. B. Wexler, G. S. Gautam and E. A. Carter, *J. Mater. Chem. A*, 2021, **9**, 9882–9897.
89 Y. Qi, Y. Liu, D. Kou, W. Zhou, Z. Zhou, Q. Tian, S. Yuan, Y. Meng and S. Wu, *ACS Appl. Mater. Interfaces*, 2020, **12**, 14213–14223.
90 X. Yu, S. Cheng, Q. Yan, J. Fu, H. Jia, Q. Sun, Z. Yang and S. Wu, *Sol. Energy Mater. Sol. Cells*, 2020, **209**, 110434.
91 B. Zhao, Y. Deng, L. Cao, J. Zhu and Z. Zhou, *Front. Chem.*, 2022, **10**, 974761.
92 C. Gao, W. Li, X. Zhou, H. Xu, Q. Zhou, H. Gao, S. Qin, Z. Gao and W. Yu, *Sol. Energy Mater. Sol. Cells*, 2023, **251**, 112147.
93 W. Ki and H. W. Hillhouse, *Adv. Energy Mater.*, 2011, **1**, 732–735.
94 S. G. Haass, M. Diethelm, M. Werner, B. Bissig, Y. E. Romanyuk and A. N. Tiwari, *Adv. Energy Mater.*, 2015, **5**, 1500712.
95 H. Xin, J. K. Katahara, I. L. Braly and H. W. Hillhouse, *Adv. Energy Mater.*, 2014, **4**, 1301823.
96 H. Xin, S. M. Vorpahl, A. D. Collord, I. L. Braly, A. R. Uhl, B. W. Krueger, D. S. Ginger and H. W. Hillhouse, *Phys. Chem. Chem. Phys.*, 2015, **17**, 23859–23866.
97 F. Martinho, S. Lopez-Marino, M. Espindola-Rodriguez, A. Hajijafarassar, F. Stulen, S. Grini, M. Dobeli, M. Gansukh, S. Engberg, E. Stamate, L. Vines, J. Schou, O. Hansen and S. Canulescu, *ACS Appl. Mater. Interfaces*, 2020, **12**, 39405–39424.
98 Y. Gong, Y. Zhang, Q. Zhu, Y. Zhou, R. Qiu, C. Niu, W. Yan, W. Huang and H. Xin, *Energy Environ. Sci.*, 2021, **14**, 2369–2380.
99 Y. Gong, R. Qiu, C. Niu, J. Fu, E. Jedlicka, R. Giridharagopal, Q. Zhu, Y. Zhou, W. Yan, S. Yu, J. Jiang, S. Wu, D. S. Ginger, W. Huang and H. Xin, *Adv. Funct. Mater.*, 2021, **31**, 2101927.
100 M. A. Green, E. D. Dunlop, J. Hohl-Ebinger, M. Yoshita, N. Kopidakis and X. Hao, *Prog. Photovolt.: Res. Appl.*, 2021, **30**, 3–12.
101 J. Wang, J. Zhou, X. Xu, F. Meng, C. Xiang, L. Lou, K. Yin, B. Duan, H. Wu, J. Shi, Y. Luo, D. Li, H. Xin and Q. Meng, *Adv. Mater.*, 2022, **34**, 2202858.
102 L. Huang, S. Wei and D. Pan, *ACS Appl. Mater. Interfaces*, 2018, **10**, 35069–35078.
103 A. Cabas-Vidani, S. G. Haass, C. Andres, R. Caballero, R. Figi, C. Schreiner, J. A. Márquez, C. Hages, T. Unold, D. Bleiner, A. N. Tiwari and Y. E. Romanyuk, *Adv. Energy Mater.*, 2018, **8**, 1801191.
104 Y. Zhao, X. Han, L. Chang, J. Li, C. Dong, Y. Fang and J. Li, *Sol. Energy Mater. Sol. Cells*, 2018, **179**, 427–434.
105 J. Zhang, B. Yao, Z. Ding and Y. Li, *ACS Appl. Energy Mater.*, 2022, **5**, 11740–11747.
106 F. Yang, X. Dong, L. Yu, X. Sun, J. Chen, Y. Zhao and Y. Li, *ACS Appl. Energy Mater.*, 2022, **5**, 11431–11440.
107 X.-F. Dong, T.-T. Zheng, F.-X. Yang, X.-D. Sun, L. Yu, J.-T. Chen, C.-W. Wang, Y. Zhao and Y. Li, *Sol. Energy Mater. Sol. Cells*, 2021, **227**, 111102.
108 S. Ge, H. Gao, R. Hong, J. Li, Y. Mai, X. Lin and G. Yang, *ChemSusChem*, 2019, **12**, 1692–1699.
109 C.-J. Hsu, H.-S. Duan, W. Yang, H. Zhou and Y. Yang, *Adv. Energy Mater.*, 2014, **4**, 1301287.
110 Y. Sun, S. Qin, D. Ding, H. Gao, Q. Zhou, X. Guo, C. Gao, H. Liu, Y. Zhang and W. Yu, *Chem. Eng. J.*, 2022, 140596.
111 F. Liu, S. Shen, F. Zhou, N. Song, X. Wen, J. A. Stride, K. Sun, C. Yan and X. Hao, *J. Mater. Chem. C*, 2015, **3**, 10783–10792.
112 C. Niu, Y. Gong, R. Qiu, Q. Zhu, Y. Zhou, S. Hao, W. Yan, W. Huang and H. Xin, *J. Mater. Chem. A*, 2021, **9**, 12981–12987.
113 Y. Cui, M. Wang, P. Dong, S. Zhang, J. Fu, L. Fan, C. Zhao, S. Wu and Z. Zheng, *Adv. Sci.*, 2022, **9**, 2201241.
114 H. Luan, B. Yao, Y. Li, R. Liu, Z. Ding, Y. Sui, Z. Zhang, H. Zhao and L. Zhang, *Sol. Energy Mater. Sol. Cells*, 2019, **195**, 55–62.
115 J. A. Clark, A. Murray, J. M. Lee, T. S. Autrey, A. D. Collord and H. W. Hillhouse, *J. Am. Chem. Soc.*, 2019, **141**, 298–308.
116 H. Guo, G. Wang, R. Meng, Y. Sun, S. Wang, S. Zhang, J. Wu, L. Wu, G. Liang, H. Li and Y. Zhang, *J. Mater. Chem. A*, 2020, **8**, 22065–22074.
117 H. Guo, R. Meng, G. Wang, S. Wang, L. Wu, J. Li, Z. Wang, J. Dong, X. Hao and Y. Zhang, *Energy Environ. Sci.*, 2022, **15**, 693–704.
118 K. Tanaka, N. Moritake and H. Uchiki, *Sol. Energy Mater. Sol. Cells*, 2007, **91**, 1199–1201.
119 K. Tanaka, N. Moritake, M. Oonuki and H. Uchiki, *Jpn. J. Appl. Phys.*, 2008, **47**, 598–601.
120 X. Zhao, Y. Pan, C. Zuo, F. Zhang, Z. Huang, L. Jiang, Y. Lai, L. Ding and F. Liu, *Sci. Bull.*, 2021, **66**, 880–883.
121 K. Tanaka, M. Oonuki, N. Moritake and H. Uchiki, *Sol. Energy Mater. Sol. Cells*, 2009, **93**, 583–587.
122 N. Moritake, Y. Fukui, M. Oonuki, K. Tanaka and H. Uchiki, *Phys. Status Solidi C*, 2009, **6**, 1233–1236.
123 K. Tanaka, Y. Fukui, N. Moritake and H. Uchiki, *Sol. Energy Mater. Sol. Cells*, 2011, **95**, 838–842.
124 K. Maeda, K. Tanaka, Y. Fukui and H. Uchiki, *Sol. Energy Mater. Sol. Cells*, 2011, **95**, 2855–2860.
125 G. M. Ilari, C. M. Fella, C. Ziegler, A. R. Uhl, Y. E. Romanyuk and A. N. Tiwari, *Sol. Energy Mater. Sol. Cells*, 2012, **104**, 125–130.
126 Z. Su, K. Sun, Z. Han, H. Cui, F. Liu, Y. Lai, J. Li, X. Hao, Y. Liu and M. A. Green, *J. Mater. Chem. A*, 2014, **2**, 500–509.
127 K. Zhang, Z. Su, L. Zhao, C. Yan, F. Liu, H. Cui, X. Hao and Y. Liu, *Appl. Phys. Lett.*, 2014, **104**, 141101.
128 F. Q. Zeng, Y. Q. Lai, Z. L. Han, B. K. Ng, Z. A. Zhang, H. L. Zhang, L. X. Jiang and F. Y. Liu, *RSC Adv.*, 2016, **6**, 6562–6570.
129 Z. Su, J. M. R. Tan, X. Li, X. Zeng, S. K. Batabyal and L. H. Wong, *Adv. Energy Mater.*, 2015, **5**, 1500682.
130 S.-H. Wu, C.-W. Chang, H.-J. Chen, C.-F. Shih, Y.-Y. Wang, C.-C. Li and S.-W. Chan, *Prog. Photovolt.: Res. Appl.*, 2017, **25**, 58–66.

131 S.-H. Wu, K.-T. Huang, H.-J. Chen and C.-F. Shih, *Sol. Energy Mater. Sol. Cells*, 2018, **175**, 89–95.
132 Z. Su, G. Liang, P. Fan, J. Luo, Z. Zheng, Z. Xie, W. Wang, S. Chen, J. Hu, Y. Wei, C. Yan, J. Huang, X. Hao and F. Liu, *Adv. Mater.*, 2020, **32**, 2000121.
133 U. Farooq, U. A. Shah, M. Ishaq, J.-G. Hu, S. Ahmed, S. Chen, Z.-H. Zheng, Z.-H. Su, P. Fan and G.-X. Liang, *Chem. Eng. J.*, 2023, **451**, 139109.
134 K. F. Tai, D. Fu, S. Y. Chiam, C. H. Huan, S. K. Batabyal and L. H. Wong, *ChemSusChem*, 2015, **8**, 3504–3511.
135 Y. T. Hsieh, Q. Han, C. Jiang, T. B. Song, H. Chen, L. Meng, H. Zhou and Y. Yang, *Adv. Energy Mater.*, 2016, **6**, 1502386.
136 Z. Xiao, H. Luan, R. Liu, B. Yao, Y. Li, Z. Ding, G. Yang, R. Deng, G. Wang, Z. Zhang, L. Zhang and H. Zhao, *J. Alloys Compd.*, 2018, **767**, 439–447.
137 A. Ibrahim, A. Guchhait, S. Hadke, H. L. Seng and L. H. Wong, *ACS Appl. Energy Mater.*, 2020, **3**, 10402–10407.
138 S. Lie, W. Li, S. W. Leow, D. M. Bishop, O. Gunawan and L. H. Wong, *Sol. RRL*, 2020, **4**, 1900521.
139 X. Chen, M. Ishaq, A. Nafees, R. Tang, Z.-H. Zheng, J.-G. Hu, Z. Su, P. Fan, G.-X. Liang and S. Chen, *J. Mater. Chem. A*, 2022, **10**, 22791–22802.
140 X. Zhao, Y. Pan, S. Liu, L. Jiang, Y. Lai and F. Liu, *Sci. China Mater.*, 2023, **66**, 895–902.
141 H. Geng, M. Wang, S. Wang, D. Kou, Z. Zhou, W. Zhou, Y. Qi, S. Yuan, L. Han, Y. Meng and S. Wu, *Adv. Funct. Mater.*, 2022, **33**, 2210551.
142 J. Zhong, Z. Xia, C. Zhang, B. Li, X. Liu, Y.-B. Cheng and J. Tang, *Chem. Mater.*, 2014, **26**, 3573–3578.
143 Q. Tian, L. Huang, W. Zhao, Y. Yang, G. Wang and D. Pan, *Green Chem.*, 2015, **17**, 1269–1275.
144 Y. Yang, G. Wang, W. Zhao, Q. Tian, L. Huang and D. Pan, *ACS Appl. Mater. Interfaces*, 2015, **7**, 460–464.
145 Y. Yang, X. Kang, L. Huang, S. Wei and D. Pan, *J. Power Sources*, 2016, **313**, 15–20.
146 X. Xu, L. Guo, J. Zhou, B. Duan, D. Li, J. Shi, H. Wu, Y. Luo and Q. Meng, *Adv. Energy Mater.*, 2021, **11**, 2102298.
147 L. Guo, J. Shi, Q. Yu, B. Duan, X. Xu, J. Zhou, J. Wu, Y. Li, D. Li, H. Wu, Y. Luo and Q. Meng, *Sci. Bull.*, 2020, **65**, 738–746.
148 K. Yin, X. Xu, M. Wang, J. Zhou, B. Duan, J. Shi, D. Li, H. Wu, Y. Luo and Q. Meng, *J. Mater. Chem. A*, 2022, **10**, 779–788.
149 Q. Tian, H. Lu, Y. Du, J. Fu, X. Zhao, S. Wu and S. Liu, *Sol. RRL*, 2018, **2**, 1800233.
150 J. A. Clark, A. R. Uhl, T. R. Martin and H. W. Hillhouse, *Chem. Mater.*, 2017, **29**, 9328–9339.
151 K.-J. Yang, J.-H. Sim, D.-H. Son, Y.-I. Kim, D.-H. Kim, D. Nam, H. Cheong, S. Kim, J. Kim and J.-K. Kang, *Nano Energy*, 2017, **35**, 52–61.
152 F. Liu, Q. Zeng, J. Li, X. Hao, A. Ho-Baillie, J. Tang and M. A. Green, *Mater. Today*, 2020, **41**, 120–142.
153 M. He, J. Huang, J. Li, J. S. Jang, U. P. Suryawanshi, C. Yan, K. Sun, J. Cong, Y. Zhang, H. Kampwerth, M. P. Suryawanshi, J. Kim, M. A. Green and X. Hao, *Adv. Funct. Mater.*, 2021, **31**, 2104528.
154 C. Yan, K. Sun, J. Huang, S. Johnston, F. Liu, B. P. Veettil, K. Sun, A. Pu, F. Zhou, J. A. Stride, M. A. Green and X. Hao, *ACS Energy Lett.*, 2017, **2**, 930–936.
155 J. Márquez, H. Stange, C. J. Hages, N. Schaefer, S. Levcenko, S. Giraldo, E. Saucedo, K. Schwarzburg, D. Abou-Ras, A. Redinger, M. Klaus, C. Genzel, T. Unold and R. Mainz, *Chem. Mater.*, 2017, **29**, 9399–9406.
156 J. Zhou, X. Xu, B. Duan, H. Wu, J. Shi, Y. Luo, D. Li and Q. Meng, *Nano Energy*, 2021, **89**, 106405.
157 Z.-K. Yuan, S. Chen, H. Xiang, X.-G. Gong, A. Walsh, J.-S. Park, I. Repins and S.-H. Wei, *Adv. Funct. Mater.*, 2015, **25**, 6733–6743.
158 M. G. Gang, V. C. Karade, M. P. Suryawanshi, H. Yoo, M. He, X. Hao, I. J. Lee, B. H. Lee, S. W. Shin and J. H. Kim, *ACS Appl. Mater. Interfaces*, 2021, **13**, 3959–3968.
159 T. Enkhbat, E. Enkhbayar, M. H. Sharif, M. S. Mina, S. Song and J. Kim, *ACS Appl. Mater. Interfaces*, 2021, **13**, 45426–45434.
160 T. J. Huang, X. Yin, G. Qi and H. Gong, *Phys. Status Solidi RRL*, 2014, **08**, 735–762.
161 S.-Y. Kim, D.-H. Son, Y.-I. Kim, S.-H. Kim, S. Kim, K. Ahn, S.-J. Sung, D.-K. Hwang, K.-J. Yang, J.-K. Kang and D.-H. Kim, *Nano Energy*, 2019, **59**, 399–411.
162 S.-Y. Kim, S.-H. Kim, D.-H. Son, Y.-I. Kim, S. Kim, S.-J. Sung, K.-J. Yang, D.-H. Kim and J.-K. Kang, *ACS Appl. Mater. Interfaces*, 2020, **12**, 46037–46044.
163 S.-Y. Kim, S.-H. Kim, D.-H. Son, H. Yoo, S. Kim, S. Kim, Y.-I. Kim, S.-N. Park, D.-H. Jeon, J. Lee, H.-J. Jo, S.-J. Sung, D.-K. Hwang, K.-J. Yang, D.-H. Kim and J.-K. Kang, *ACS Appl. Mater. Interfaces*, 2022, **14**, 30649–30657.
164 B. Duan, L. Guo, Q. Yu, J. Shi, H. Wu, Y. Luo, D. Li, S. Wu, Z. Zheng and Q. Meng, *J. Energy Chem.*, 2020, **40**, 196–203.
165 Y. Hou, H. Azimi, N. Gasparini, M. Salvador, W. Chen, L. S. Khanzada, M. Brandl, R. Hock and C. J. Brabec, *ACS Appl. Mater. Interfaces*, 2015, **7**, 21100–21106.
166 F. Liu, S. Wu, Y. Zhang, X. Hao and L. Ding, *Sci. Bull.*, 2020, **65**, 698–701.
167 F. Martinho, S. Lopez-Marino, M. Espíndola-Rodríguez, A. Hajijafarassar, F. Stulen, S. Grini, M. Döbeli, M. Gansukh, S. Engberg, E. Stamate, L. Vines, J. Schou, O. Hansen and S. Canulescu, *ACS Appl. Mater. Interfaces*, 2020, **12**, 39405–39424.
168 C. W. Hong, S. W. Shin, M. P. Suryawanshi, M. G. Gang, J. Heo and J. H. Kim, *ACS Appl. Mater. Interfaces*, 2017, **9**, 36733–36744.
169 X. Liu, Y. Feng, H. Cui, F. Liu, X. Hao, G. Conibeer, D. B. Mitzi and M. Green, *Prog. Photovolt.: Res. Appl.*, 2016, **24**, 879–898.
170 I. Sharma, P. S. Pawar, R. K. Yadav, R. Nandi and J. Heo, *Sol. Energy*, 2022, **246**, 152–180.
171 Y. Xue, B. Yu, W. Li, S. Feng, Y. Wang, S. Huang, C. Zhang and Z. Qiao, *Superlattices Microstruct.*, 2017, **112**, 311–317.

172 X. Qin, B. Xu, J. Lin, J. Chen, H. Tong, Y. Chen, P. Yang, J. Chu and L. Sun, *Sol. Energy Mater. Sol. Cells*, 2022, **242**, 111781.
173 B. Xu, X. Qin, X. Lu, Y. Liu, Y. Chen, H. Peng, P. Yang, J. Chu and L. Sun, *Sol. RRL*, 2021, **5**, 2100216.
174 S. Chen, A. Walsh, X. G. Gong and S. H. Wei, *Adv. Mater.*, 2013, **25**, 1522–1539.
175 S. Kim, J.-S. Park and A. Walsh, *ACS Energy Lett.*, 2018, **3**, 496–500.
176 C. J. Hages, A. Redinger, S. Levcenko, H. Hempel, M. J. Koeper, R. Agrawal, D. Greiner, C. A. Kaufmann and T. Unold, *Adv. Energy Mater.*, 2017, **7**, 1700167.
177 S. Ma, H. Li, J. Hong, H. Wang, X. Lu, Y. Chen, L. Sun, F. Yue, J. W. Tomm, J. Chu and S. Chen, *J. Phys. Chem. Lett.*, 2019, **10**, 7929–7936.
178 W. Chen, D. Dahliah, G.-M. Rignanese and G. Hautier, *Energy Environ. Sci.*, 2021, **14**, 3567–3578.